Thermodynamic and Structural Analysis of Microtubule Assembly: The Role of GTP Hydrolysis

Bojana Vulevic and John J. Correia
Department of Biochemistry, University of Mississippi Medical Center, Jackson, Misssippi 39216 USA

ABSTRACT Different models have been proposed that link the tubulin heterodimer nucleotide content and the role of GTP hydrolysis with microtubule assembly and dynamics. Here we compare the thermodynamics of microtubule assembly as a function of nucleotide content by van't Hoff analysis. The thermodynamic parameters of tubulin assembly in 30–100 mM piperazine-*N,N'*-bis(2-ethanesulfonic acid), 1 mM $MgSO_4$, 2 mM EGTA, pH 6.9, in the presence of a weakly hydrolyzable analog, GMPCPP, the dinucleotide analog GMPCP plus 2 M glycerol, and GTP plus 2 M glycerol were obtained together with data for taxol-GTP/GDP tubulin assembly (GMPCPP and GMPCP are the GTP and GDP nucleotide analogs where the $\alpha\beta$ oxygen has been replaced by a methylene, $-CH_2-$). All of the processes studied are characterized by a positive enthalpy, a positive entropy, and a large, negative heat capacity change. GMPCP-induced assembly has the largest negative heat capacity change and GMPCPP has the second largest, whereas GTP/2 M glycerol- and taxol-induced assembly have more positive values, respectively. A large, negative heat capacity is most consistent with the burial of water-accessible hydrophobic surface area, which gives rise to the release of bound water. The heat capacity changes observed with GTP/2 M glycerol-induced and with taxol-induced assembly are very similar, -790 ± 190 cal/mol/K, and correspond to the burial of 3330 ± 820 Å^2 of nonpolar surface area. This value is shown to be very similar to an estimate of the buried nonpolar surface in a reconstructed microtubule lattice. Polymerization data from GMPCP- and GMPCPP-induced assembly are consistent with buried nonpolar surface areas that are 3 and 6 times larger. A linear enthalpy-entropy and enthalpy-free energy plot for tubulin polymerization reactions verifies that enthalpy-entropy compensation for this system is based upon true biochemical correlation, most likely corresponding to a dominant hydrophobic effect. Entropy analysis suggests that assembly with GTP/2 M glycerol and with taxol is consistent with conformational rearrangements in 3–6% of the total amino acids in the heterodimer. In addition, taxol binding contributes to the thermodynamics of the overall process by reducing the $\Delta H°$ and $\Delta S°$ for microtubule assembly. In the presence of GMPCPP or GMPCP, tubulin subunits associate with extensive conformational rearrangement, corresponding to 10% and 26% of the total amino acids in the heterodimer, respectively, which gives rise to a large loss of configurational entropy. An alternative, and probably preferable, interpretation of these data is that, especially with GMPCP-tubulin, additional isomerization or protonation events are induced by the presence of the methylene moiety and linked to microtubule assembly. Structural analysis shows that GTP hydrolysis is not required for sheet closure into a microtubule cylinder, but only increases the probability of this event occurring. Sheet extensions and sheet polymers appear to have a similar average length under various conditions, suggesting that the minimum cooperative unit for closure of sheets into a microtubule cylinder is approximately 400 nm long. Because of their low level of occurrence, sheets are not expected to significantly affect the thermodynamics of assembly.

INTRODUCTION

The mechanism of microtubule assembly has been extensively studied. Earlier work stressed the isolation of the primary component, tubulin, and microtubule-associated proteins (MAPs), with a focus on in vitro polymerization conditions (reviewed in Kirschner, 1978; Timasheff and Grisham, 1980; Correia and Williams, 1983). A critical need for GTP was established, and the GTP exchangeable binding site (E-site), located on the β-subunit of the tubulin heterodimer, has been shown to be the site of hydrolysis and an energetic link to microtubule assembly and microtubule dynamics (Geahlen and Haley, 1979). An early theory of assembly identified a difference in stability at the two microtubule ends, which causes a difference in critical concentration and in rates of growth, and thus gives rise to treadmilling, a net addition of subunits at one end and a net loss of subunits at the other end (Margolis and Wilson, 1978). It is now known that microtubules exist in a dynamic equilibrium with tubulin subunits, called dynamic instability, in which microtubules at both ends oscillate between growing and shrinking phases (Mitchison and Kirschner, 1984; Horio and Hotani, 1986). Mitchison and Kirschner (1984) originally proposed that microtubule ends were stabilized by a layer of GTP-liganded tubulin molecules that capped the unstable GDP-microtubule lattice. It was established that GTP hydrolysis closely follows the addition of the tubulin subunits to the end of a microtubule, and only a few GTP-containing subunits at the tip are sufficient to stabilize a growing microtubule (Carlier et al., 1987; Stewart et al., 1990; Martin et al., 1993; Drechsel and Kirchner,

Received for publication 23 September 1996 and in final form 13 December 1996.

Address reprint requests to Dr. John J. Correia, Department of Biochemistry, University of Mississippi Medical Center, 2500 North State St., Jackson, MS 39216-4505. Tel.: 601-984-1522; Fax: 601-984-1501; E-mail: jcorreia@fiona.umsmed.edu.

0006-3495/97/03/1357/19 $2.00

1994; Caplow and Shanks, 1996). A weakly hydrolyzable GTP analog, GMPCPP, and a nonhydrolyzable analog, GMPPCP, have been shown to suppress dynamic instability and provide further direct evidence that microtubule dynamics are regulated by GTP hydrolysis (Caplow, 1992; Hyman et al., 1992; Caplow et al., 1994; Dye and Williams, 1996). (GMPCPP and GMPCP are the GTP and GDP nucleotide analogs where the $\alpha\beta$ oxygen has been replaced by a methylene, $-CH_2-$.)

Conformational changes related to assembly-disassembly of microtubules have been proposed to occur after hydrolysis of GTP (Howard and Timasheff, 1986; Melki et al., 1989; Mandelkow et al., 1991). These conformational end points tend to be described as the "straight" conformation, corresponding to the straight protofilament in the microtubule cylinder, and the "curved" conformation, corresponding to a ring (Howard and Timasheff, 1986) or a curled protofilament at the end of a microtubule (Mandelkow et al., 1991). These conformations, while actually quaternary designations, are generally associated with either GTP or GDP bound to the tubulin E-site, respectively, and reflect the strength of lateral interaction between subunits (Melki and Carlier, 1993; Vernier et al., 1994). A microtubule "straight" protofilament within the GDP-tubulin core represents a constrained conformation and is the driving force for disassembly in dynamic instability (Caplow et al., 1994). The structural features of GMPCPP-microtubules, a putative GTP-like lattice, were suggested to come from either a change in lateral bonding between GTP-like subunits (Vale et al., 1994) or a change in the packing density along the protofilaments (Hyman et al., 1995). It has recently been proposed that GTP hydrolysis is triggered in a growing microtubule by a "curved" to "straight" conformational change at the ends of microtubules as GTP-tubulin sheet extensions close into a microtubule lattice (Chretien et al., 1995). Variability in the rate of microtubule growth and shrinkage is proposed to coincide with variation in the rate of sheet extension and cylinder closure.

The most fundamental way of investigating the nature of the interactions responsible for macromolecular polymer formation is by thermodynamic analysis (Wyman and Gill, 1990). There have been extensive van't Hoff and calorimetric studies on the thermodynamics of tubulin assembly under various ligand and buffer conditions (Frigon and Timasheff, 1975a,b; Sutherland and Sturtevant, 1976; Lee and Timasheff, 1977; Hinz et al., 1979; Johnson and Borisy, 1979; Johnson, 1980; Berkowitz et al., 1980; Andreu et al., 1983; Melki and Carlier, 1993; Diaz et al., 1993). However, a quantitative thermodynamic study of the contribution of GTP hydrolysis to the assembly reaction has not been conducted. Our goal here is to use thermodynamic analysis and electron microscopy to study the linkage between microtubule formation and GTP hydrolysis by comparing assembly in the presence of a weakly hydrolyzable GTP analog, GMPCPP, with GTP-induced assembly.

MATERIALS AND METHODS

Reagents

Deionized (Nanopure) water was used in all experiments. $MgSO_4$, EGTA, GDP (type I), GTP (type II-S), glycerol, and piperazine-*N,N'*-bis(2-ethanesulfonic acid) (PIPES) were all purchased from Sigma Chemical Company. Taxol was provided by the National Cancer Institute.

Synthesis of GMPCP and GMPCPP

GMPCP and GMPCPP were synthesized in our laboratory as described by Hyman et al. (1992), with modifications as described below. (A more detailed synthesis is available upon request.) We used initial compounds in amounts corresponding to a quarter of that described by Hyman et al. (1992). A mixture of pyridine, tributylamine, and methylene diphosphonic acid was warmed at 60°C in a rotary evaporator until the methylene diphosphonic acid was dissolved. Isopropylidene guanosine and dicyclohexylcarbodiimide were added and reacted at 60°C for 6 h, during which dicyclohexylurea separated as a fine precipitate. The reaction was followed by thin-layer chromatography (TLC) using silica gel IB2-F (Baker) and a chloroform:methanol:acetic acid (80:20:2, v/v) solvent. Isopropylene guanosine has an r_f of 0.6, and the product stays at the origin. The reaction mix was evaporated using a Rotovap and resuspended in 50 ml water. After filtering through a Buchner funnel, and washing the cake with water, the filtrate was adjusted to pH 7 and extracted five times with diethylether. The solution was then evaporated and resuspended in water twice, and finally resuspended in 10% acetic acid. Note that this mixture should not be allowed to sit overnight. To deprotect and remove the isopropylidene group, the mixture was incubated at 100°C for 2 h. The reaction was monitored by TLC on PEI-cellulose-F (Baker) plates with a 1.4 M LiCl solvent. GMPCP has an r_f of 0.5, and isopropylidene-GMPCP stays at the origin. After evaporating and resuspending the mixture in water four times (to remove the acetic acid), the pellet was resuspended in 40 ml water and the pH was adjusted to 8.5 with NaOH. Diethylether extractions were carried out until clear (five times), and the excess ether was blown off with a stream of nitrogen. The precipitate was decanted and loaded on a 400-ml DE 52 (Whatman) column (5 × 20 cm). The column was eluted with a 2-liter gradient of 0–0.2 M triethylamine bicarbonate (TEAB), pH 7.0–7.5, followed by a 2-liter 0.2–0.4 M TEAB gradient (340 drop fractions). The GMPCP peak at the start of the second gradient was pooled, dried down, resuspended in methanol twice, resuspended in minimal water, and then passed over an AG 50W X2 (BioRad) column, saturated with NaOH to obtain the Na^+ form without a TEA residue (unlike in the Hyman procedure). A typical yield is 450 mg from a quarter prep.

To convert GMPCP to GMPCPP, GMPCP was first dissolved in 50 mM Tris, 10 mM β-mercaptoethanol, 10 mM $MgSO_4$, pH 7.5. The solution was made 20 mM in acetylphosphate, and 10–20 μg/ml of acetate kinase (Sigma) was added. The mixture was incubated at room temperature for 48 h, while adjusting the pH every 8 h. At 24 h, additional acetylphosphate (5 mM) and acetate kinase were added if needed. The reaction was monitored by TLC on PEI-cellulose-F plates; GMPCP r_f = 0.5, GMPCPP r_f = 0.2. There should be a 90% conversion to product. The solution was then loaded on a DE 52 column and eluted with a 0–0.3 M and a 0.3–0.6 M TEAB gradient. GMPCPP was pooled, dried, resuspended, converted to Na^+ form by passing over the AG 50W X2 column, and lyophylized. A typical yield is 90% by TLC, but only 60% by actual starting material. GMPCP and GMPCPP were stored at −20°C as dry powder or a 50 mM H_2O stock. The purity and identity of both GMPCP and GMPCPP was established to be 99% by high-performance liquid chromatography on a SynChropak AX-300 anion exchange column as described (Correia et al., 1987) and by H NMR (performed by David Graves, Department of Chemistry, University of Mississippi).

Tubulin purification

MAP-free pig tubulin was purified by two warm/cold polymerization cycles followed by phosphocellulose (PC) chromatography, as described

by Williams and Lee (1982) and modified by Correia et al. (1987). Protein concentrations were determined spectrophotometrically (ϵ_{278} = 1.2 L/g-cm; Detrich and Williams, 1978). Tubulin was in general equilibrated into the appropriate buffer by column centrifugation (Penefsky, 1977). Note that the equilibration of tubulin with GMPCP, GMPCPP, and GDP takes advantage of the Mg^{2+} dependence of GTP binding by equilibrating tubulin into a Mg^{2+}-free buffer to completely remove exchangeable GTP at the E-site. This procedure allows the relatively easy production of 99% GDP-tubulin in a single step. Then GDP-tubulin is equilibrated by column centrifugation into the appropriate buffer (30–100 mM PIPES, 1 mM $MgSO_4$, 2 mM EGTA, 1 mM GXP (guanine nucleotide of the appropriate form)). Glycerol (2 M) in the appropriate buffer is added at this stage, before degassing; taxol is added at 1:1 after degassing.

Turbidity measurements

Polymerization of PC-tubulin (tubulin purified by phosophocellulose chromatography) was monitored using a Gilford Response II UV-VIS scanning spectrophotometer equipped with a Peltier cell holder. Tubulin solutions at various concentrations and in buffers with various ligand compositions (30–100 mM PIPES, 1 mM $MgSO_4$, 2 mM EGTA, 1 mM GXP, ±2 M glycerol) were degassed for 30 min on ice. The first baseline data were obtained at 4°C and at 350 nm. The temperature was increased to the desired temperature and solutions were monitored at 350 nm until plateau values are obtained. Solutions were then cooled to 0°C to verify cold sensitivity and to record the second baseline if possible. The change in optical density between the second baseline and the plateau value was plotted against tubulin concentration, and the critical concentration was obtained from the x axis intercept. Data from 10–15 separate experiments were combined to determine the critical concentration. For taxol-stimulated assembly, the reaction in general was not rapidly or completely cold sensitive, and thus the change in optical density between the first baseline and the plateau value was used.

There has been great concern in the literature about complete nucleotide exchange before polymerization studies (Diaz et al., 1993; Caplow et al., 1994). Under our conditions we can prepare 99% GDP-tubulin or GTP-tubulin in a single step (Correia et al., 1987). However, because of the relatively low affinity of GMPCPP and GMPCP reported for the E-site relative to GDP (Caplow et al., 1994), simple addition of analog might be insufficient for polymerization studies. To verify that the addition of 1 mM analog is sufficient, we performed a series of polymerizations in 2 M glycerol, 0.1 M PIPES, 1 mM Mg^{2+}, 2 mM EGTA, pH 6.9, at 10 μM GDP-tubulin with the addition of 10–1000 μM GMPCPP. Turbidity plateaued by 250 μM GMPCPP, and at 10 μM analog the turbidity reached 71% of the plateau value. This suggests that simple addition of analog is sufficient to compete with GDP and promote microtubule assembly. Thus analog binding is coupled to polymerization and easily competes with GDP as long as enough GMPCPP-tubulin is initially present to nucleate assembly. This suggests that equilibration by column centrifugation should be more than sufficient to promote microtubule assembly. To verify this, samples were prepared by making GDP-tubulin and then equilibrated twice by column centrifugation into 1 mM GMPCP or 1 mM GMPCPP plus 100 mM PIPES, 1 mM $MgSO_4$, 2 mM EGTA, pH 6.9. Polymerizations were conducted at 37°C, and the C_r estimates were compared with values determined from our standard procedures (see Tubulin Purification, above, and Fig. 3). The values agreed to within 0.1 μM in C_r and strongly suggest that our conditions give reliable estimates of C_r values. This is further supported by our observation that in 2 M glycerol the critical concentration with GMPCPP at temperatures of >10°C is unmeasurable and identical to zero, implying 100% exchange.

In principle, similar studies are possible with the nonhydrolyzable analogs GMPPCP and GMPPNP. The advantage of using GMPCPP over GMPPCP or GMPPNP resides in their relative affinity for the E-site. GMPPCP and GMPPNP have affinities much less than 1×10^5 M^{-1}, which thus requires the use of alkaline phosphatase or charcoal to remove GTP/GDP from the site to allow their binding. Otherwise these nonhydrolyzable analogs do not successfully compete with the endogenous GTP or GDP nucleotide and thus the GMPPCP- or GMPPNP-tubulin concentration is too low to nucleate. This led to an earlier disagreement over the importance of GTP hydrolysis in the reaction mechanism (Seckler et al., 1990). Alternatively, GMPCPP-Mg binds with high enough affinity (estimated to be 3×10^6 M^{-1}; Caplow et al., 1994) to exchange for GDP at the E-site. (Note that Caplow's values are relative to earlier estimates of GTP affinity that did not properly correct for Mg^{2+} dependence and thus are low by at least a factor of 2 (Correia et al., 1987). We have verified that GMPCPP and GMPCP bind Mg^{2+} with the same affinity as GTP and GDP (Correia et al., 1987).) We further take advantage of the low affinity of GTP in the absence of Mg^{2+} to ensure that the competition is between GMPCPP-Mg or GMPCP-Mg and GDP-Mg ($K = 2.6 \times 10^7$ M^{-1}).

Thermodynamic analysis of assembly

To calculate thermodynamic parameters from experimental data, critical concentrations were obtained by extrapolation of turbidity values at different protein concentrations to zero turbidity (Berne, 1974). The critical concentration C_r was converted to an association constant, K_p (Gaskin et al., 1974; Lee and Timasheff, 1977), by

$$K_p = 1/C_r,$$

and ln K_p was plotted versus the temperature at which the sample was incubated. Data were fitted to the truncated van't Hoff equation (Glasstone, 1947)

$$\ln K_p = A + B^*(1/T) + C^*\ln T$$

using the FITALL program (MTR software, Toronto, Canada). Thermodynamic parameters are estimated by the following equations:

$$\Delta G^\circ = -RT \ln K_p$$

$$\Delta H^\circ = R(C^*T - B)$$

$$\Delta S^\circ = (\Delta H^\circ - \Delta G^\circ)/T$$

$$\Delta C_p^\circ = R^*C.$$

Monte Carlo simulations

Fitting the experimental points to the integrated van't Hoff equation (Glasstone, 1947) gives thermodynamic parameters that are prone to large uncertainties. To check if this is due to incorrect error analysis in the FITALL routine used or limitations of the fitting problem (e.g., highly correlated parameters), we performed Monte Carlo simulations (Correia and Yphantis, 1992; Correia and Chaires, 1994) using a computer program MCTIM created in our laboratory. The parameters obtained by fitting the set of experimental data with FITALL were used to create "perfect" ln K_p data according to the van't Hoff equation over the range and number of experimental temperature values. Random noise corresponding to the standard deviation of the best fit of the experimental ln K_p data was added to the "perfect" ln K_p set, and the "noisy" data were fit by a nonlinear least-squares (NLS) routine to the van't Hoff equation. (The use of the same standard deviation for all data points in a set is reasonable here because the experimental error on each C_r and ln K_p value is approximately constant because of the ability to raise or lower the protein concentration to obtain comparable signals or change in turbidity, $\Delta\tau$.) The thermodynamic parameters and their standard deviation were calculated and saved, the old noise removed, a new noise set added, and the process repeated. After 1000 such fits, the thermodynamic parameter files were analyzed for the mean and standard deviation (Correia and Yphantis, 1992; Correia and Chaires, 1994). This file of thermodynamic parameters reflects the information content of the van't Hoff data set and provides an estimate of the uncertainty or standard deviation of the energetics. As expected, the uncertainty depends linearly upon the magnitude of the noise and is

dependent upon the square root of the number of experimenal points (data not shown). The distributions are also analyzed for their skew, a measure of symmetry, and their kurtosis, a measure of peakedness of the distribution (Correia and Chaires, 1994). Note that to be statistically different from a Gaussian distribution, the skew and the kurtosis must be larger than the absolute value of $(6/n)^{1/2}$ and $(24/n)^{1/2}$, respectively, where n is the number of samples. For 1000 cases the expected skew and kurtosis are ± 0.077 and ± 0.155.

In Fig. 1, we see a typical distribution of ΔC_p, $\Delta S°$ and $\Delta H°$ for the case of GMPCP-tubulin polymerization. All three distributions have approximately a Gaussian shape, as indicated by the values of the skew and kurtosis. Thus, of the examples in Fig. 1, *A* shows a symmetrical distribution with a flattened peak, and both panel *B* and *C* show a slightly skewed distribution with a typical Gaussian kurtosis. Similar analysis was performed for each data set, and the resulting standard deviations are listed in Table 1 as $\pm$ values. Parameters are often highly correlated with each other. A typical way to evaluate this is a correlation plot (Correia and Chaires, 1994) in which the estimates for one parameter are plotted versus another for all simulated cases. The cross-correlation coefficient is indicated by the distribution or randomness of the data. A typical case corresponding to GMPCP-2 M glycerol-induced assembly is shown in Fig. 2. The enthalpy and entropy changes are seen to be highly linearly correlated,

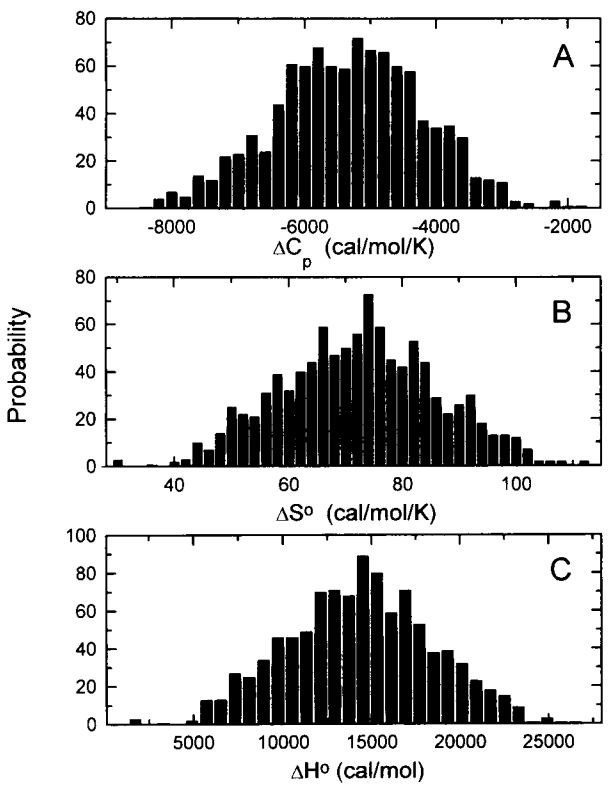

FIGURE 1 Evaluation of the fitting of 1000 cases of noisy data to the integrated van't Hoff equation for the GMPCP-tubulin polymerization experiment. The parameters and the appropriate noise level are listed in Table 1. (*A*) Probability, derived from the number of occurrences, that a particular ΔC_p value is the best fitted value, plotted versus the actual ΔC_p value in cal/mol/K. This distribution has a skew of 0.021 and a kurtosis of -0.099. (*B*) Probability, derived from the number of occurrences, that a particular ΔS value is the best fitted value, plotted versus the actual ΔS value in cal/mol/K. This distribution has a skew of a 0.051 and a kurtosis of -0.120. (*C*) Probability, derived from the number of occurrences, that a particular ΔH value is the best fitted value, plotted versus the actual ΔH value in cal/mol. This distribution has a skew of a 0.051 and a kurtosis of -0.121.

with an R value of 0.99996 (Fig. 2 *A*), whereas the changes in entropy, or enthalpy, with respect to changes in heat capacity show a lower but still significant level of correlation, with an R value of -0.80697 or -0.80177, respectively (Fig. 2 *B*). The enthalpy-entropy correlations are typically this large (0.99974 $\pm$ 0.00015), whereas the $\Delta H°$ and $\Delta S°$ versus ΔC_p correlations are usually much smaller (-0.2855 ± 0.422). As the data in Fig. 2 *A* are derived from a Monte Carlo simulation, the high degree of correlation is a mathematical artifact due to significant cross-correlation coefficients and demonstrates the difficulty in independently determining $\Delta H°$ and $\Delta S°$ values. Note that the slope of the $\Delta H°$-$\Delta S°$ plot, 299.5 K, is essentially the harmonic mean of the experimental data. Krug et al. (1976a,b,c) pointed out that this is diagnostic of a mathematical, nonchemical correlation. Alternatively, a plot of $\Delta H°$ versus $\Delta G°$ (Fig. 2 *C*) is not linearly correlated, with an R value of only -0.2325 for this case, and averaging 0.028 ± 0.343 for all nine cases simulated (see Table 1). This is consistent with the suggestion that true chemical correlation must be evaluated by a plot of ΔH versus ΔG (Krug et al., 1976a,b,c).

Electron microscopy

Samples in different tubulin polymerization conditions (0.3–5.8 mg/ml tubulin in 0.1 M PIPES, 1 mM $MgSO_4$, 2 mM EGTA, pH 6.9, 1 mM GXP, with/without 2 M glycerol) were degassed for 30 min and polymerized at 22°C or 36°C for 30–45 min in the Gilford Response II UV-VIS scanning spectrophotometer, and samples were taken for electron microscopy examination. Samples were diluted 1:10–1:15 with a glutaraldehyde/buffer solution (1% final glutaraldehyde concentration) and left at room temperature for 1 min. Copper grids (200 mesh; Polysciences, Inc.) were prepared with 0.25% (w/v) polyvinyl formal solutions in ethylene dioxide and carbon coated. The procedure for specimen preparation was described by Vonck and van Bruggen (1990). Grids were laid on the top of a 10-μl drop of sample/glutaraldehyde solutions for 1 min, then washed with two drops of water and negatively stained for 2 min with 1% uranyl acetate. This temporal procedure minimizes structural distortions to the microtubule lattice (Cross and Williams, 1991). Grids were examined and photographed at 5000× magnification with a Zeiss EM 10 electron microscope. Prints were made (8 inches × 10 inches) at threefold magnification (3 M Dry Silver Paper; Ted Pella, Inc).

Measurement of tubulin polymer lengths

The lengths of tubulin polymers were obtained by collecting the data from photographs using a digitizing tablet with Sigma-Scan 3.9 software (Jandel Scientific). Sheet polymers or sheet extensions could easily be visualized as low-contrast structures by negative stain. By "sheet polymer" we mean that the lattice was 100% open, whereas a sheet extension was connected to a microtubule cylinder of dark contrast. A microtubule with a sheet extension is referred to as a mixed polymer. Sheet extensions are typically found at the end of a microtubule cylinder and only rarely in the middle of a microtubule cylinder. A microtubule cylinder of dark contrast can exist as part of a mixed polymer or as a 100% closed microtubule lattice. For analysis of total length and percentage of polymerized tubulin in microtubule cylinders versus sheet lattice, we measured the length of all single polymers visible on the grid. Bundles were ignored because of the inability to resolve sheets or closed lattice types. Length distribution analysis and percentage of sheet or microtubule lattice in a mixed polymer lattice involved measurements of polymers, the ends of which are both visible. Statistical analysis of length distribution data was performed in Origin (Microcal Software, Inc).

RESULTS

Temperature dependence of guanine nucleotide and ligand-induced polymerization

To understand the role of guanine nucleotide hydrolysis in microtubule assembly, we performed turbidimetry experi-

TABLE 1 Thermodynamic parameters of tubulin assembly obtained from van't Hoff analysis

Ligand	Buffer*	ΔC_p° (cal/mol/K)	ΔG° (cal/mol)	ΔH° (cal/mol)	ΔS° (cal/mol/K)	Noise level
GMPCPP	100 mM PIPES	−1512 ± 865	−7931 ± 77	16542 ± 2863	82 ± 9	0.30
GMPCPP	75 mM PIPES	−2286 ± 309	−7935 ± 25	16577 ± 975	82 ± 3	0.12
GMPCPP	50 mM PIPES	−2770 ± 859	−7382 ± 47	21166 ± 2480	95 ± 8	0.20
GMPCP	100 mM PIPES 2 M glycerol	−5284 ± 1130	−7383 ± 37	13918 ± 4114	71 ± 14	0.18
GTP	100 mM PIPES 2 M glycerol	−790 ± 230	−6728 ± 22	11255 ± 754	60 ± 3	0.09
GTP	75 mM PIPES 2 M glycerol	−625 ± 321	−6409 ± 24	11547 ± 1125	60 ± 4	0.10
GTP	50 mM PIPES 2 M glycerol	−1083 ± 529	−6100 ± 24	12868 ± 3272	63 ± 11	0.06
GTP	10 mM phosphate# 3.4 M glycerol 1 mM EGTA 16 mM Mg^{2+}, pH 7.0	−1500 ± 500	−6652	16160	76	NR
Taxol, GTP	30 mM PIPES	−545 ± 256	−7067 ± 27	6133 ± 896	44 ± 3	0.14
Taxol, GTP	PEDTA§	0 ± 71	−7082	11379	61	NR
Taxotere, GTP	PEDTA§	0 ± 71	−7404	12338	66	NR
Taxol, GDP	30 mM PIPES	−915 ± 319	−6690 ± 29	5079 ± 1074	39 ± 4	0.13
Taxol, GDP	PEDTA§	0 ± 71	−6389	11727	60	NR
Taxotere, GDP	PEDTA§	0 ± 71	−6884	12042	63	NR
$ZnCl_2$, GTP	Buffer A¶	−1400 ± 100	−8354	12000	68	NR
$ZnCl_2$, GTP	Buffer A¶	−1200 ± 100	−7923	14024	73	NR
Colchicine/GTP	10 mM phosphate‖ 1 mM EGTA 16 mM Mg^{2+}, pH 7.0	−1200	−6000	31923	126	0.13
$MgCl_2$, GTP	PG buffer**	135 ± 48	−5828	4193	33	0.008
GTP, MAPs	PMG buffer##I	0	−6207	9100	51	NR
GTP, MAPs	PMG buffer##II	0	−7007	8000	50	NR
GTP, MAPs	PMG buffer##III	0	−8025	46000	180	NR
Fish brain, GTP	PMG buffer§§	0	−9817	26500	121	NR
Fish egg, GTP	PMG buffer§§	0	−11421	33900	151	NR

*1 mM [GXP], 1 mM $MgSO_4$, 2 mM EGTA, pH 6.9; turbidimetry experiments unless indicated otherwise. All data reported at the mean harmonic temperature (27°C).

#Data from Lee and Timasheff (1977).

§10 mM phosphate, 1 mM EDTA, 4 mM $MgCl_2$, pH 6.7 data from Diaz et al. (1993).

¶100 mM MES, 30% glycerol, 150 μM $ZnCl_2$, 150 μM GXP, pH 6.8; data from Melki and Carlier (1993).

‖Data from Andreu et al. (1983).

**10 mM sodium phosphate, 16 mM $MgCl_2$, pH 7.0; analytical ultracentrifugation experiments from Frigon and Timasheff (1975).

##0.1 M PIPES, 0.1 mM $MgCl_2$, pH 6.9; I) species concentrations determined by sedimentation assay, II) turbidity experiments >20°C, III) turbidity experiments <20°C; data from Johnson and Borisy (1979).

§§0.1 M PIPES, 2 mM $MgSO_4$, 1 mM GTP, pH 6.82; from Detrich et al. (1992).

NR, not reported.

ments to obtain propagation constants K_p for microtubule formation (Lee and Timasheff, 1977). The temperature dependences of GMPCPP, GMPCP-2 M glycerol, and GTP-2 M glycerol tubulin assembly was compared to the GTP-3.4 M glycerol data from Lee and Timasheff (1977) and are presented as a van't Hoff plot (Fig. 3). (The Lee and Timasheff (1977) data are used here as the standard reference for the thermodynamics of microtubule assembly and were performed in a 10 mM phosphate, 1 mM GTP, 16 mM Mg^{2+}, 1 mM EGTA, 3.4 M glycerol, pH 7.0 buffer.) The thermodynamic parameters for each data set were determined by fitting to the truncated van't Hoff equation and are listed in Table 1 at the mean harmonic temperature, 27°C (Krug et al., 1976a,b,c). The errors are estimated by Monte Carlo simulation as described in Materials and Methods. (For the purpose of direct comparison, Table 1 also contains the results for all other tubulin self-association reactions studied by van't Hoff analysis (see below).) Van't Hoff analysis of the nine microtubule polymerization conditions investigated yields excellent estimation of the enthalpy and entropy change, ±16% and ±10% error, respectively. However, the heat capacity change is more poorly estimated, with a average error of ± 37%, although five of the cases have approximately a 26% error. (Note that 33% is the estimated error for ΔC_p by Lee and Timasheff (1977), and taken together with our Monte Carlo simulations seems to be a typical error for van't Hoff analysis.) The cases with the largest error in ΔC_p in general have the smallest curvature, and/or span a smaller temperature range and thus also have fewer points.

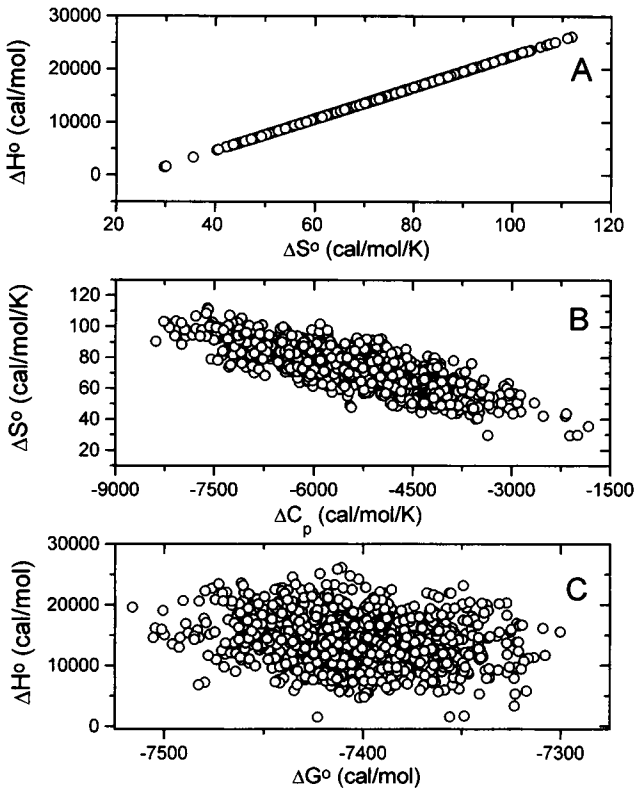

FIGURE 2 Relationship between thermodynamic parameters for 1000 cases of simulated GMPCP-tubulin polymerization data shown in Fig. 3. (*A*) Enthalpy change $\Delta H°$ (cal/mol) of simulated cases plotted versus entropy change $\Delta S°$ (cal/mol/K). The slope of a linear fit, the compensation temperature, is 299.4 K with a linear correlation coefficient R value of 0.99996. The average value for the nine cases simulated for Table 1 was 299.9 ± 1.4. (*B*) Entropy change $\Delta S°$ (cal/mol/K) of simulated cases plotted versus heat capacity change ΔC_p (cal/mol/K) ($R = -0.80697$). A similar plot is obtained for $\Delta H°$ versus ΔC_p ($R = -0.80177$; data not shown). These are rather large degrees of correlation, with typical absolute values being −0.295 ± 0.443. (*C*) Enthalpy change $\Delta H°$ (cal/mol) of simulated cases plotted versus free energy change $\Delta G°$ (cal/mol) ($R = -0.2325$). The average absolute value of correlation observed was 0.028 ± 0.343.

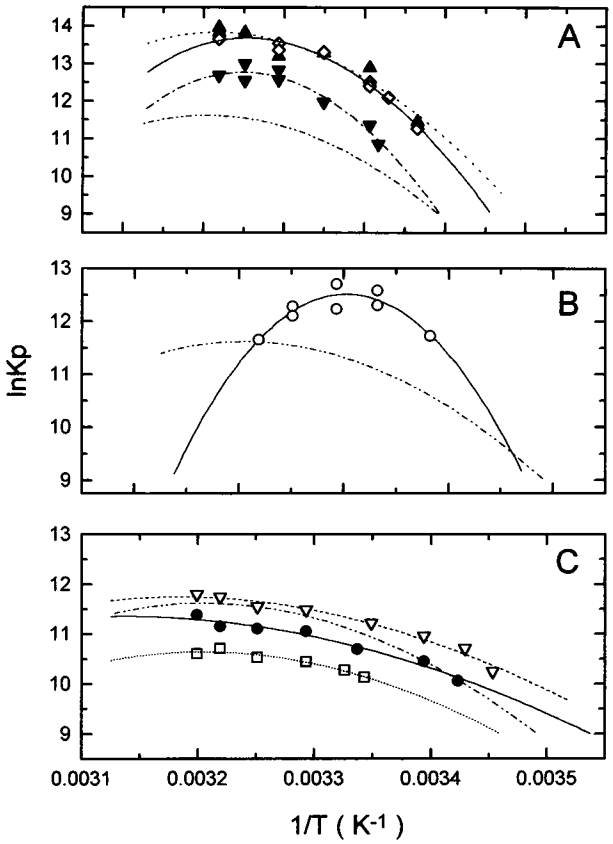

FIGURE 3 Van't Hoff plot of nucleotide-induced microtubule polymerization. The - · · - line in each panel corresponds to GTP-tubulin in 3.4 M glycerol data taken from Lee and Timasheff (1977). The other lines correspond to best fits of the corresponding data to the integrated van't Hoff equation. (*A*) GMPCPP-tubulin in 1 mM $MgSO_4$, 2 mM EGTA, pH 6.9 (▲), 100 mM PIPES; ◇, 75 mM PIPES; ▼, 50 mM PIPES. (*B*) GMPCP-tubulin (○) in 2 M glycerol, 1 mM $MgSO_4$, 2 mM EGTA, 100 mM PIPES, pH 6.9. (*C*) GTP-tubulin in 2 M glycerol, 1 mM $MgSO_4$, 2 mM EGTA, pH 6.9. ▽, 100 mM PIPES; ●, 75 mM PIPES; □, 50 mM PIPES.

For GMPCPP-induced polymerization (Fig. 3 *A*), the critical concentration C_r is lower and the propagation constant ln K_p is increased relative to GTP-2 M glycerol-induced assembly. The extent of polymerization is also observed to decrease with decreasing ionic strength. (Glycerol was omitted from the GMPCPP buffer because in its presence the C_r was too small and ln K_p too large to be measurable. Below 50 mM PIPES and in the absence of glycerol, the C_r was too large to be easily obtained.) Microtubule polymerization in the presence of GMPCPP is characterized by positive enthalpy, positive entropy, and negative heat capacity (Table 1). These parameters are comparable to the results of Lee and Timasheff (1977), and at 100 mM PIPES they are virtually identical. There is a decrease in heat capacity (a larger negative number) with decreasing ionic strength, although within error the estimates are not significantly different (2190 ± 520 or 23.7%).

Lee and Timasheff (1977) used tubulin purified by a method different from ours (Williams and Lee, 1982) in a buffer containing 3.4 M glycerol. To evaluate our results with GMPCPP and more closely compare them with the data of Lee and Timasheff (1977), we performed experiments with PC-tubulin in a similar series of GTP-2 M glycerol-containing buffers. The level of polymerization in GTP-2 M glycerol (Fig. 3 *C*) is similar to that observed by Lee and Timasheff (1977) and is characterized by a positive enthalpy and entropy change and a negative heat capacity change. These data are less curved than the GMPCPP data and the Lee and Timasheff data (Fig. 3, *A* and *C*), and the fits thus result in a more positive change in heat capacity. As with GMPCPP-induced assembly, the extent of polymerization with GTP-2 M glycerol exhibits a slight decrease with decreasing ionic strength, consistent with electrostatic repulsion between tubulin subunits and less productive microtubule polymerization (Serrano et al., 1984). (This is presumably why in the 10 mM PO_4 buffer system of Lee

and Timasheff (1977) 16 mM $MgCl_2$ is required to stimulate assembly.)

During microtubule assembly the half-time for GMPCPP hydrolysis is reported to be 9.5 h (Hyman et al., 1992), and thus we have no significant generation of GMPCP-tubulin during the time of these experiments. However, this reduced rate of hydrolysis suggests that the $\alpha\beta$-methylene in GMPCPP might contribute to alteration of the tubulin conformation and reduction of GTPase activity. Thus we tested the ability of the GDP analog GMPCP to induce microtubule assembly, exploring the hypothesis that the $\alpha\beta$-methylene might favor a more GTP-like tubulin conformation. In the absence of glycerol, no polymerization was observed up to 5 mg/ml tubulin concentration. However, in the presence of 2 M glycerol reversible microtubule formation was observed, although data were only obtainable over a limited temperature range in 100 mM PIPES buffer (Fig. 3 *B*). The dinucleotide form of the analog enhances assembly 3.5-fold over the GTP-3.4 glycerol data of Lee and Timasheff (1977), although the level of GMPCP-polymerization is 2.5-fold less than with the trinucleotide analog at the same ionic strength. As with GMPCPP and GTP-2 M glycerol, GMPCP-2 M glycerol-induced assembly was characterized by a positive enthalpy and entropy change and a negative heat capacity change. However, a pronounced curvature of the van't Hoff plot was observed, leading to an extremely large estimate of the ΔC_p for GMPCP-induced polymerization, -5284 ± 1130 cal/mol/K (Table 1). It is not clear if this is due to a narrower range of data or to a real change in the heat capacity of the system (see Discussion).

The taxoid anticancer drugs, taxol and taxotere, have the unusual property of inducing microtubule formation. Diaz et al. (1993) have performed extensive van't Hoff analysis of taxol- and taxotere-induced microtubule assembly in the presence of GDP and GTP. They observed a positive change in enthalpy and entropy that was similar to our results. In contrast to GTP- and GMPCPP-induced assembly, they observed a straight van't Hoff plot characteristic of no change in heat capacity. Because Diaz et al. (1993) also worked with tubulin purified by a different procedure in a 10 mM PO_4, 4 mM $MgCl_2$, pH 6.7 buffer, we elected to repeat the experiments with taxol in a 30 mM PIPES, 1 mM $MgSO_4$, 2 mM EGTA, pH 6.9 buffer with PC purified tubulin. (This buffer was chosen because it is similar to our polymerization buffer and because it gave an extent of assembly comparable to the data of Diaz et al. (1993).) In Fig. 4 we present van't Hoff analysis of taxol-induced assembly of GTP- and GDP-tubulin (Fig. 4, *A* and *B*, respectively). In both cases we compared our results to data taken from Diaz et al. (1993) for taxol and taxotere. The K_p for taxol-induced assembly in the presence of GTP is approximately twofold larger than that for GDP-tubulin, whereas Diaz et al. (1993) report a similar increase of threefold in the presence of GTP. Our data appear to be similar to those of Diaz et al. (1993), but the fitted lines, in our case, exhibit slight curvature. This curvature corresponds to a significant change in heat capacity, -915 and -545 cal/mol/K for GDP and GTP conditions, respectively (Table 1), compared to no change in ΔC_p found in the work by Diaz et al. (1993). Note the $\Delta H°$ and $\Delta S°$ data from Diaz et al. (1993) are surprisingly similar to the GTP-2 M glycerol data at 27°C (Table 1), whereas the presence of curvature in our taxol data gives rise to a significantly smaller $\Delta H°$ and $\Delta S°$ value for both conditions.

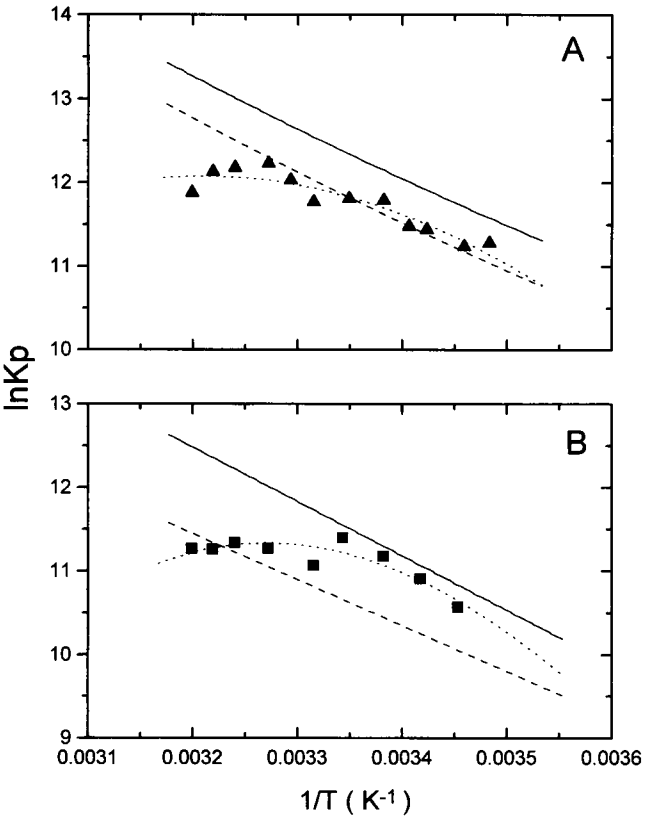

FIGURE 4 Van't Hoff plot of taxoid induced microtubule polymerization. The dotted lines correspond to best fits of the corresponding data to the integrated van't Hoff equation. (*A*) ▲, GTP-tubulin in taxol, 1 mM $MgSO_4$, 2 mM EGTA, 30 mM PIPES, pH 6.9. ·····, Best fit of the data; ——, corresponds to GTP-tubulin in taxotere data from Diaz et al. (1993); – – –, corresponds to GTP-tubulin in taxol data from Diaz et al. (1993). (*B*) (■) GDP-tubulin in taxol, 1 mM $MgSO_4$, 2 mM EGTA, 30 mM PIPES, pH 6.9. ——, Corresponds to GDP-tubulin in taxotere data from Diaz et al. (1993); – – –, corresponds to GDP-tubulin in taxol data from Diaz et al. (1993).

Enthalpy-entropy compensation analysis

To obtain a better understanding and comparison of the thermodynamic parameters obtained from the polymerization in the presence of various nucleotides, we performed $\Delta H°$-$\Delta S°$ and $\Delta H°$-$\Delta G°$ compensation analysis. In Fig. 5 *A*, a plot of enthalpy-entropy compensation, evaluated at the mean harmonic values of the experimental data (*squares*), shows an extremely high linear correlation. Surprisingly, all published van't Hoff data for tubulin self-association (*circles, triangles*) demonstrate a similar linear correlation (Fig. 5 *A*). Krug et al. (1976a,b,c) investigated the statistical

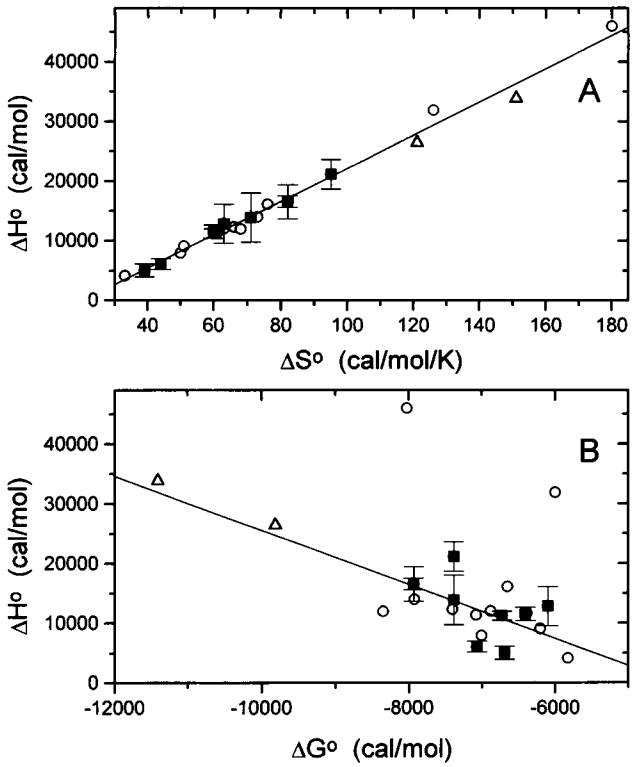

FIGURE 5 Relationship at mean harmonic temperature between enthalpy change for microtubule polymerization, $\Delta H°$ (cal/mol), and other thermodynamic parameters. The closed squares correspond to the experimental data (Table 1) collected for this paper; GMPCPP-tubulin in 100 mM PIPES, 75 mM PIPES, 50 mM PIPES; GMPCP-tubulin in 100 mM PIPES; GTP-2 M glycerol-tubulin in 100 mM PIPES, 75 mM PIPES, 50 mM PIPES; GTP-taxol tubulin in 30 mM Pipes; GDP-taxol tubulin in 30 mM Pipes. The open circles correspond to the remaining data in Table 1 taken from other studies of bovine or porcine tubulin polymerization. The open triangles correspond to microtubule assembly with Antarctic fish tubulins. (*A*) $\Delta H°$ versus the entropy change for microtubule polymerization, $\Delta S°$ (cal/molK). The solid line is a fit to all data plotted (■, ○, △) and has a slope of 278.1 ± 6.3, with an R value 0.99471. A fit of the experimental data in this paper (■) has a slope of 277.1 ± 11.4, with an R value of 0.99417 (data not shown). (*B*) $\Delta H°$ versus free energy change of microtubule polymerization, $\Delta G°$ (cal/mol). The solid line is a linear fit to all of the data, excluding the two outliers corresponding to MAP- and colchicine-induced assembly (■, ○, △), and has an R value of 0.84787.

problems associated with the analysis of van't Hoff data and suggested a comparison of data at the mean harmonic temperature to avoid edge effects in the fitting and nonchemical correlation between $\Delta H°$ and $\Delta G°$. They also assert that for enthalpy-entropy compensation to be statistically significant, the slope of the $\Delta H°$-$\Delta S°$ plot, i.e., the correlation temperature or T_c, should have a value different from the experimental temperature at which the enthalpy and entropy change was calculated. The slope of the $\Delta H°$-$\Delta S°$ plot of the nine experimental points collected in this work (*squares*) is 277.1 ± 11.4 K or 4.0°C, a value significantly different from the experimental temperature, 27°C. The slope of the plot for all tubulin self-association data (*squares, circles, triangles*) is 278.1 ± 6.3 K, or 5.0°C, a value that is also significantly different from 27°C by the criteria described by Krug et al. (1976a,b,c). (This is to be contrasted with the simulated Monte Carlo data (see Fig. 2 *A*), where the average slope, 299.9 ± 1.4 K, is the harmonic mean temperature, and the correlation observed is a mathematical, nonchemical correlation.) Thus, by this criterion, we can conclude that these data exhibit statistically reliable enthalpy-entropy compensation. This suggests that all of the tubulin self-association reactions summarized in Table 1 and Fig. 5 *A* reflect similar protein-protein interactions.

An additional and more convincing means of evaluating whether this is real compensation or a statistical artifact is to plot enthalpy versus free energy (Krug et al., 1976a,b,c), shown in Fig. 5 *B*. The $\Delta H°$ versus $\Delta G°$ plot for the experimental data reported here (*squares*) also shows a moderate degree of correlation with a linear correlation coefficient of 0.52 (fitted line, not shown). Excluding the two points due to taxol-stimulated assembly increases the linear correlation to 0.65 (fitted line, not shown). Thus, relative to the uncorrelated behavior seen between $\Delta H°$ versus $\Delta G°$ in Monte Carlo simulations (Fig. 2 *C*), this degree of correlation in the experimental data suggests that the enthalpy-entropy compensation in the case of nucleotide- or taxol-induced microtubule polymerization is a real biochemical phenomenon. Furthermore, a similar $\Delta H°$ versus $\Delta G°$ plot is obtained for all of the data from Table 1 (Fig. 5 *B*, *squares, circles, triangles*), excluding two outliers, and corresponds to a linear correlation coefficient of 0.85. The two outliers correspond to MAP-induced microtubule assembly below 20°C (Johnson and Borisy, 1979; Johnson, 1980) and colchicine-induced assembly (Andreu et al., 1983). In the case of MAP-induced assembly below 20°C, the MAPs are proposed to bind to the dissociating protofilaments, stabilize MAP-tubulin polymer structures, and increase the off rate (Johnson and Borisy, 1979). Thus the $\Delta H°$ and $\Delta G°$ measured under these conditions are not exclusively indicative of the reversible binding of tubulin to the growing microtubule, but include a contribution from MAP binding. For colchicine-induced assembly, the $\Delta H°$ and $\Delta G°$ measured may also reflect an inhibitory contribution caused by colchicine binding (Andreu et al., 1983). (We have no explanation of why a similar argument does not apply to taxoid-induced assembly.) It is interesting that the $\Delta H°$ and $\Delta S°$ are still well correlated for both cases, consistent with the more stringent utility of the $\Delta H°$-$\Delta G°$ plot. Note that the tubulin polymerization data summarized in Table 1 and Fig. 5 are not typical of the data compared by Krug et al. (1976a,b,c), because they correspond to various solution conditions and polymerization reactions (collected in different laboratories) rather than the effect of simple chemical modification of a single compound. Thus we conclude that despite the high degree of statistical correlation possible in van't Hoff analysis, as verified and demonstrated by Monte Carlo analysis, the data collected in this paper and the majority of data collected on tubulin self-association appear to exhibit statistically reliable enthalpy-entropy compensation and enthalpy-free energy correlation. A similar observation has been made for actin filament formation

(Swezey and Somero, 1982, 1985; see Discussion). As discussed by Andreu et al. (1983) for colchicine-induced assembly, the remarkable similarity in the thermodynamic characteristics of these tubulin self-assembly reactions, i.e. $+\Delta H$, $+\Delta S$, $-\Delta C_p$, suggest a common mechanism that is driven by similar protein-protein and protein-solvent interactions. Note that Ha et al. (1989) suggest the observation of a large negative heat capacity ($\Delta C_p \ll 0$) is consistent with enthalpy-entropy compensation. The enthalpy-entropy compensation observed and verified here further demonstrates that changes in nucleotide content contribute to the thermodynamics of the process.

Structural studies of tubulin polymer in different nucleotide and ligand conditions

The thermodynamic analysis of microtubule assembly presented above suggests that all solution conditions lead to the same or similar polymer forms, which contain the same or similar interaction interfaces. To verify the formation of microtubule polymers, EM observations of negatively stained samples were observed between 30 and 45 min after initial warming. This guaranteed that the thermodynamics and the structural studies were correlated. Under all solution conditions studied, microtubules were the predominant polymer observed, although open or sheet-like polymers were evident, especially in the GMPCPP samples. This is of interest because Chretien et al. (1995) have proposed a linkage between GTP hydrolysis and the closure of sheet-like extension off growing microtubules into a microtubule cylinder. They suggest that variable rates of closure may regulate the variable rate of microtubule growth observed by video-enhanced DIC (differential interference contrast microscopy) (Gildersleeve et al., 1992). Although the results of Chretien et al. (1995) are based on kinetic experiments, they suggest that microtubules grown with a nonhydrolyzable analog, GMPCPP, may have a greater tendency to form sheets than microtubules. This hypothesis is based upon the energetic argument that if microtubule closure affects GTP hydrolysis, GTP hydrolysis affects microtubule closure (Wyman, 1964). To test this hypothesis we performed length distribution analysis on microtubules grown with GMPCPP, GMPCP-2 M glycerol, and GTP-2 M glycerol (Table 2). Experiments were performed at 36°C and 22°C to ensure that the results pertained to the entire span of the van't Hoff studies. Results were quantified to compare the percentage of total length that was in a sheet structure and in a microtubule cylinder. GTP-2 M glycerol-induced assembly gave identical results at 36°C and 22°C, 2.4% (±0.1%) sheet, whereas GMPCPP-induced assembly was equally consistent at both temperatures, 6.9% (±0.1%). GMPCP-2 M glycerol-induced assembly gave results that were expected for a GDP analog, 0.8% and 1.1% sheet at 22°C and 36°C, respectively. To ensure these results were not biased by the absence of glycerol in the GMPCPP samples, the experiments were repeated with GMPCPP-2 M glycerol and with GTP in the absence of glycerol (Table 2). GTP-induced assembly gave results similar to that in the

TABLE 2 Measurements of microtubule cylinder, sheet extension, and sheet polymer lengths for different tubulin assembly conditions

Tubulin* assembly	% of polymer length in sheet	Number of polymers#	Mean length of microtubule polymer§ (nm)	% of polymers that are mixed polymers	Mean length of mixed polymer (nm)	Mean length of sheet extension (nm)	% of polymers that are sheet polymers	Mean length of sheet polymer (nm)
GMPCPP assembly								
22°C	6.8	979	1229 ± 698	12.3	1489 ± 693	412 ± 238	7.1	464 ± 435
36°C	7.0	649	1063 ± 695	18.0	1274 ± 829	298 ± 148	7.4	276 ± 199
22°C, glycerol								
30 min	28.9	723	657 ± 355	24.0	850 ± 361	339 ± 210	19.6	357 ± 180
150 min	22.9	438	991 ± 530	30.4	1117 ± 491	445 ± 249	17.1	406 ± 169
660 min	15.1	407	1073 ± 605	28.0	1351 ± 560	424 ± 211	7.8	504 ± 218
1440 min	11.8	356	1428 ± 938	30.8	1705 ± 857	498 ± 216	2.5	447 ± 223
36°C, glycerol								
30 min	32.6	693	618 ± 450	21.2	972 ± 492	373 ± 258	26.1	529 ± 326
150 min	7.2	467	765 ± 439	11.5	977 ± 537	308 ± 136	1.9	464 ± 192
GMPCP assembly								
22°C + glyc.	0.8	466	2934 ± 2467	10.3	2569 ± 2318	212 ± 210	0.8	238 ± 200
36°C + glyc.	1.1	585	2885 ± 2413	5.3	2019 ± 2008	363 ± 430	3.2	439 ± 263
GTP assembly								
36°C	1.7	625	2938 ± 3083	7.7	3020 ± 4677	368 ± 519	2.4	1610 ± 2321
22°C + glyc.	2.3	731	2745 ± 2732	5.5	3838 ± 3459	607 ± 644	2.3	1205 ± 1325
36°C + glyc.	2.5	543	2655 ± 2238	9.0	3576 ± 3028	525 ± 628	4.2	864 ± 681

*0.1 M PIPES, 1 mM $MgSO_4$, 2 mM EGTA, 1 mM [GXP], +/− 2 M glycerol, pH 6.9.

#Tubulin polymer is a microtubule cylinder, a microtubule cylinder with sheet extension (called a mixed polymer), or a sheet polymer only.

§Microtubule cylinder and mixed polymer.

presence of glycerol, 1.7% versus 2.4% sheet. However, GMPCPP-2 M glycerol-induced assembly at both temperatures had exceedingly high sheet content, 28.9% and 32.6% sheet at 22°C and 36°C, respectively. This is a surprising result. Even if glycerol induced GMPCPP hydrolysis (Caplow et al., 1994), polymerization with GMPCP-2 M glycerol generated exclusively (99%) closed microtubule cylinders. One possibility is that GMPCPP-2 M glycerol microtubules do not close as quickly. To test this, length distributions were measured at different times after initial warming (Table 3). After 150 min at 36°C, the percentage of lengths in sheet structures stabilized at 7.2%, whereas at 22°C the percentage of lengths in sheet had only dropped to 22.9%. After 11 h at 22°C the percentage dropped to 15.1%, whereas at 24 h it was only down to 11.8%. Thus GMPCPP-2 M glycerol-induced polymerization at 22°C exhibits a slow closure rate, and the rate of closure exhibits an activation energy that can be partially overcome by raising the temperature to 36°C.

One difference in the experimental conditions compared above is the efficiency of nucleation leading to a much shorter length distribution with GMPCPP-induced versus GMPCP- or GTP-induced assembly. The GMPCPP-2 M glycerol-induced microtubules at 30 min are, on average, 657 to 618 nm long at 22°C and 36°C respectively, whereas the GMPCP-2 M glycerol-induced microtubules are, on average, 2–3 μm long, and the GTP-2 M glycerol-induced microtubules are 3–4 μm long. It is possible that closure of sheets into microtubules is a cooperative process that requires or prefers a minimum length. During the 22°C time course experiment, the average polymer length of GMPCPP-2 M glycerol microtubules was observed to increase from 657 to 1428 nm, presumably by annealing, because very little dynamic instability is anticipated in these experiments. Surprisingly, the mean length of the sheetlike extensions or the 100% sheet polymers did not change and exhibited a fairly constant length of 428 ± 60 nm. What changed was the length of microtubule cylinder, either in mixed polymers or in 100% microtubule lattice polymers. Similar observations were made in the 36°C time course data. In fact, with the exception of the GTP-2 M glycerol-induced sheetlike polymers, the average sheet extension or sheet polymer length, based on 13 experimental conditions or time points and 23 different distributions, was 404 ± 99 nm. This clearly suggests a preferred or cooperative length for closure of a sheet into a microtubule. (Note that at 36°C the distributions are in general identical by a two-parameter Student's *t*-test, whereas at 22°C the distributions are in general not identical. Thus although the average lengths of sheets are very similar, the differences may reflect other kinetic or structural factors. We do not suggest that there is a strong energetic dependency upon sheet length above a minimum length and thus we are not surprised by broad distributions.) This length corresponds to approximately 50 tubulin heterodimers along a single protofilament and 657 heterodimers in a 13-protofilament structure. Thus, assembly with a nonhydrolyzable analog, GMPCPP, does appear to weakly favor an open sheet structure, although the preference is kinetically mediated by the temperature and the length distribution, or nucleation efficiency, of the conditions. Note, however, that these results further demonstrate only 0.9–6.9% of the total length in these polymers is an open structure under the conditions used for thermodynamic studies (Table 2), and thus suggest that these small differences will not significantly contribute to differences in turbidity or differences in thermodynamics.

DISCUSSION

In the present work we used thermodynamic and structural analysis for the purpose of investigating the relationship between self-assembly, GTP hydrolysis, and conformational changes in microtubule polymers. Using Monte Carlo simulation, we established that enthalpy and entropy changes estimated from van't Hoff analysis are accurate to approximately ±16% and ±10%, respectively, whereas the ΔC_p estimates can only be determined to approximately ±26% under the best circumstances. This limitation is due in part to the narrow temperature range over which tubulin is stable and can be reversibly polymerized. Under the best conditions, i.e., taxol- or GMPCPP-stimulated assembly, this temperature range is approximately 15–42°C. In most other cases in this work and in many previous studies (Table 1), the temperature range is 10°C narrower. In addition, accurate estimation of thermodynamic parameters is limited by parameter correlations reflected by large cross-correlation coefficients, as demonstrated by highly linear ΔH-ΔS correlation plots (Fig. 2 *A*; Correia and Chaires, 1994), and by the presence of curvature, usually due to ΔC_p, in the van't Hoff plot. For the extreme case, i.e., $\Delta C_p < |\pm 200|$ cal/mol/K, ΔC_p estimation by van't Hoff analysis is an ill-posed fitting problem (Chaires, 1996). The standard deviations observed in our study are, in general, typical of errors observed in other microtubule assembly studies (Lee and Timasheff, 1977; see Table 1) and of errors observed in other van't Hoff analyses (Ha et al., 1989). (This suggests that the error estimates for ΔC_p by Melki and Carlier (1993) for Zn^{2+}-induced tubulin sheet formation derived from van't Hoff analysis, ±100 cal/mol/K corresponding to ±7.1–8.3% (see Table 1), are greatly underestimated.) Calorimetric determinations of ΔC_p, in general, are reliable to 10–20% (Hinz et al., 1979; Baldwin, 1986). Using ΔH-ΔS and ΔH-ΔG compensation analysis (Fig. 5), we established that the thermodynamic parameters estimated in this manuscript and by other workers in the field reflect, within error, real biochemical behavior. Deciphering and parsing the biochemical origin of the observed changes in thermodynamic parameters with changes in nucleotide content, ligand binding, or solution environment is the challenge we now address.

It is well established that microtubules in vivo and in vitro exhibit dynamic instability, with variable rates of growth and disassembly (Mitchison and Kirschner, 1984;

TABLE 3 Entropic contributions to tubulin association

Buffer and ligand condition*	$-\Delta C_p$[#] (cal/molK)	T_s[§] (K)	$\Delta S_{HE}(T_S)$[¶] (cal/molK)	ΔS_{rt}[‖] (cal/molK)	$-\Delta S_{other}$[**] (cal/molK)	$R^{th}\Pi$
GMPCPP 100 mM PIPES	1512	317	398 ± 228	−50	348 ± 228	62 ± 41
GMPCPP 75 mM PIPES	2286	317	602 ± 81	−50	552 ± 81	99 ± 16
GMPCPP 50 mM PIPES	2770	317	729 ± 226	−50	679 ± 226	121 ± 40
GMPCP 100 mM PIPES 2 M glycerol	5284	317	1391 ± 298	−50	1341 ± 298	239 ± 53
GTP 100 mM PIPES 2 M glycerol	790	317	208 ± 61	−50	158 ± 61	28 ± 11
GTP 75 mM PIPES 2 M glycerol	625	317	165 ± 85	−50	115 ± 85	20 ± 15
GTP 50 mM PIPES 2 M glycerol	1083	317	285 ± 139	−50	235 ± 139	42 ± 25
GTP 3.4 M glycerol 10 mM phosphate[##]	1500	317	395	−50	345	62
taxol, GTP, 30 mM PIPES	545	317	143 ± 67	−50	93 ± 67	17 ± 12
taxol, GDP, 30 mM PIPES	915	317	240 ± 84	−50	191 ± 84	34 ± 15
$ZnCl_2$, GTP[§§]	1400	317	369	−50	319	57
$ZnCl_2$, GDP[§§]	1200	317	316	−50	266	47
colchicine 10 mM Phosphate GTP tubulin[¶¶]	1200	317	316	−50	266	47
16 mM $MgCl_2$ PG Buffer GTP tubulin[‖‖]	−135	227	−97	−50	−147	−26***

*1 mM $MgSO_4$, 2 mM EGTA, 1 mM [GXP] pH 6.9, unless indicated otherwise.
[#]Data from Table 1.
[§]$T = T_S = 317.6 \pm 7.7$ at $\Delta S = 0$, (Spolar and Record, 1994).
[¶]$\Delta S_{HE}(T_s) = 1.35\Delta C_p \ln(T_s/386)$ (Spolar and Record, 1994).
[‖]As defined in Spolar and Record (1994).
**Calculated for protein association from the relationship $\Delta S(T_S) = 0 = \Delta S_{HE}(T_S) + \Delta S_{rt} + \Delta S_{other}$ (Spolar and Record, 1994).
[##]Data from Lee and Timasheff (1977).
[§§]Data from Melki and Carlier (1993).
[¶¶]Data from Andreu et al. (1983).
[‖‖]Data from Frigon and Timasheff (1975b).
***Corresponds to an order-disorder transition upon ring formation.
$\Pi R^{th} = \Delta S_{other}/-5.6$ (Spolar and Record, 1994).

Horio and Hotani, 1986; Gildersleeve et al., 1992). It is also well established that various factors suppress dynamics. These include MAPs, glycerol, taxol, and nonhydrolyzable analogs (Kowalski and Williams, 1993; Hyman et al., 1992). Thus, in the experiments conducted here, we expect either complete suppression of or diminished dynamics. Taxol-induced assembly with GDP and experiments with GMPCP in 2 M glycerol should be devoid of dynamic

instability because these are equilibrium polymers, i.e., there is no irreversible step due to GTP hydrolysis. Experiments with GMPCPP are typically at plateau by 30–45 min, well before the half-time for hydrolysis of GMPCPP, i.e., 9.5 h (Hyman et al., 1992). Thus GMPCPP-induced polymers should also be approximately equilibrium polymers. In the experiments with taxol-GTP-induced polymerization or GTP-2 M glycerol-induced polymerization, GTP hydrolysis is occurring. However, we also expect suppression of dynamics by the stabilizing action of taxol or glycerol. Thus dynamic instability should make no contribution to the measured parameters, and these parameters should reflect pseudothermodynamic equilibrium, analogous to the previous studies of Lee and Timasheff (1977) and Diaz et al. (1993).

Interpretation of thermodynamic parameters for microtubule assembly

All of the van't Hoff plots collected in this work were nonlinear. Curvature in van't Hoff analysis can have numerous causes. The primary cause is a heat capacity change, thermodynamically described as $(\partial\Delta H/\partial T)_p$ or $(T)(\partial\Delta S/\partial T)_p$. Lee and Timasheff (1977) ascribed the large negative heat capacity they observed for microtubule assembly primarily to release of water upon burial of water-accessible surface area (ASA). The hydrophobicity of the buried surface area is a major factor in this contribution (Ha et al., 1989; Spolar et al., 1989), although further analysis has indicated a significant contribution from the burial of the polar surface as well (Spolar et al., 1992; Spolar and Record, 1994). Curvature can also be due to the effect of coupled reactions, as described in detail by Eftink et al (1983). Gaskin et al. (1974) suggested that the curvature was due to a gross conformational change in the microtubule lattice, thus implying a coupled reaction possibly triggered by GTP hydrolysis. Conformational changes in secondary or tertiary structure that induce the burial of nonpolar or polar water-accessible surface area will also contribute to ΔC_p (Spolar et al., 1992; Spolar and Record, 1994). Johnson and Borisy observed a break in their van't Hoff curve at 20°C (Johnson and Borisy, 1979; Johnson, 1980) due to the formation of oligomeric complexes with MAPs below 20°C that enhanced the off rate by disassembly of MAP-stabilized oligomers. This also constitutes a coupled reaction, although MAPs are not present in the PC-tubulin utilized in experiments presented here. In addition, it has been suggested that a contribution from changes in internal dynamic or vibrational modes should contribute 20% of the heat capacity change (Sturtevant, 1977). Subsequent analysis has neglected this contribution because it is smaller than the error in ΔC_p (Baldwin, 1986; Ha et al., 1989; Spolar et al., 1989), and more recent analysis suggests that changes in vibrational modes are negligible and do not contribute to ΔC_p (Murphy et al., 1990; Spolar and Record, 1994). Thus release of water upon burial of both nonpolar and polar water-accessible surface area, coupled reactions, and conformational changes should all contribute to curvature of a van't Hoff plot.

The thermodynamic analysis presented in Table 1 shows that microtubule assembly is an entropy-driven process (below 44°C, see Table 3) with a large negative heat capacity change under both hydrolyzable and nonhydrolyzable conditions. This is true in the presence of glycerol, colchicine, or taxol. This is, in general, also true for other tubulin self-association processes in the presence of MAPs, Zn^{2+}, or Mg^{2+} (Table 1). This implies that tubulin self-assembly is qualitatively driven by similar forces, regardless of changes in the microtubule polymer lattice formed or the occurrence of GTP hydrolysis. A large negative heat capacity change is consistent with the burial of nonpolar surface, the hydrophobic effect (Sturtevant, 1977; Baldwin, 1986). Utilizing data on the transfer of nonpolar solutes from water to pure liquid phases and the folding of small globular proteins, Spolar et al. (1989) demonstrated that a quantitative relationship exists between the water-accessible nonpolar surface area (ΔA_{np}) and the magnitude of ΔC_p. This verified that the dominant contribution to ΔC_p is the hydrophobic effect and established a quantitative means of estimating ΔA_{np} from ΔC_p and of estimating ΔC_p from the surface area of binding interfaces determined from x-ray crystal structures (Ha et al., 1989; Livingstone et al., 1991). Thus the loss of water upon the formation of each tubulin-tubulin contact is a process that should contribute a positive ΔH, a positive ΔS, and a negative ΔC_p due to the burial of ASA and the hydrophobic effect (Lee and Timasheff, 1977). (Note that ionic interactions may also contribute to a positive ΔH and ΔS (Ross and Subramanian, 1981). Complete quantitative analysis requires a more complex interpretation involving burial of both nonpolar and polar ASA (see below).) Quantitatively we observe a significant variation in the heat capacity change for microtubule assembly, ranging from -5284 ± 1130 cal/mol/K for assembly in GMPCP to -545 ± 256 cal/mol/K for assembly with taxol-GTP. The largest negative values are seen under nonhydrolyzable nucleotide conditions (GMPCP and GMPCPP), whereas the presence of GTP-2 M glycerol or taxol seems to reduce the heat capacity change. Unlike the data of Diaz et al. (1993; Table 1), our thermodynamic parameters for taxol-induced assembly and GTP-2 M glycerol-induced assembly are nearly identical.

Using the method of Spolar and co-workers (Spolar et al., 1989; Ha et al., 1989; Livingstone et al., 1991), we can estimate the buried ASA from the ΔC_p values in Table 1. Without an x-ray structure to determine the relative amount of nonpolar or polar buried ASA, we follow the method of Spolar et al. (Spolar et al., 1992; Spolar and Record, 1994) to estimate the ratio. These workers have shown that ΔC_p can be estimated by the following relationship: $\Delta C_p = 0.32\ \Delta A_{np} - 0.14\Delta A_p$, where ΔA refers to the change in buried nonpolar or polar ASA. Assuming $\Delta A_p/\Delta A_{np} = 0.59$, as observed for typical protein folding reactions, then $\Delta C_p = 0.24\ \Delta A_{np}$ or $\Delta A_{np} = 4.21\ \Delta C_p$. Errors in the relative

amount of nonpolar or polar buried ASA for microtubule assembly clearly propagate into ΔC_p. These assumptions will only give us a first approximation of the desired structural interpretation of the thermodynamic quantities. The relative effects should be approximately correct unless nucleotide- or ligand-induced changes in conformation or in lattice packing significantly alter the ratio of polar to nonpolar buried ASA. A 10% error in $\Delta A_p/\Delta A_{np}$ will cause a 5.9% error in ΔC_p.

For polymerization in the presence of GTP plus 2 M glycerol, we estimate an average buried nonpolar ASA of 3500 ± 800 Å^2. The trend with buffer concentration is within experimental error and thus is neglected for the moment. Although there is also a trend with nucleotide in the taxol-stimulated assembly, the ΔC_p data are remarkably similar to polymerization with 2 M glycerol, ranging from −545 to −1083 cal/mol/K, and giving an average estimate of buried nonpolar ASA of 3330 ± 820 Å^2. The standard deviation of this nonpolar ASA estimate is ±24.5%, a value comparable to the expected experimental uncertainty. We conclude that, within error, taxol-stimulated assembly and GTP-2 M glycerol-stimulated assembly give rise to identical changes in buried nonpolar ASA. Note that to achieve a comparable extent of association with taxol (GDP or GTP) at 27°C, a decrease in ΔS is compensated by a decrease in ΔH (Table 1). (The consequences of this will be discussed further in a later section.) Polymerization induced by GMPCPP gives a significantly larger estimate of buried nonpolar ASA, 9220 ± 2180 Å^2, or a 2–3 times larger estimate with similar uncertainty, ±23.7%. Given that microtubules are the predominant structure under all conditions studied (Table 2; Diaz et al., 1993), there is an additional contribution to buried nonpolar ASA in the presence of GMPCPP, possibly derived from conformational changes upon assembly (see Table 3; Spolar and Record, 1994). Alternatively, the ratio of polar to nonpolar buried ASA may be altered by GMPCPP. For example, in the extreme case in which 100% of the buried ASA was nonpolar, then $\Delta A_{np} = 3.13\ \Delta C_p$, and the estimated buried nonpolar ASA for GMPCPP-induced assembly is reduced by 26% to 6840 ± 1620 Å^2, a value reasonably consistent with the estimate based upon the Lee and Timahseff (1977) data. Surprisingly, polymerization induced by GMPCP gives an even larger estimate of buried nonpolar ASA, 22,250 ± 4,760 Å^2. Applying the extreme case of 100% nonpolar buried ASA with GMPCP-induced assembly, this would be reduced to 16,500 ± 3,540 Å^2.

What is the expected buried ASA for microtubule assembly, and what might account for these large discrepancies in estimated buried nonpolar ASA? There currently is no high-resolution x-ray structure of tubulin or of microtubules. However, a 6.5-Å map of zinc-induced tubulin sheets has been reported (Nogales et al., 1995). Using this structure as a starting point for microtubule reconstruction (K. Downing, private communication), we can model the protofilament as an elliptical cylinder of about 45 × 55 Å cross section and, estimating the mean cross-sectional radius as 25 Å, we calculate the intersubunit contact along a protofilament to be about 1963 Å^2 per monomer. This is doubled to account for the total buried surface per subunit. The area between protofilaments is much harder to model, because the protofilaments barely touch in a reconstruction. This is consistent with large holes in the microtubule wall that accommodate taxol binding (Nogales et al., 1995). It is also consistent with weaker interactions between protofilaments than along protofilaments. Estimating a 15-Å strip between protofilaments with contacts in about half this surface gives 300 Å^2 per monomer. This corresponds to 1200 Å^2 per subunit for contacts on two adjacent protofilament. Thus the estimate for total buried surface ΔA_T is 5126 Å^2. This is reasonably close to the 6318 ± 2100 Å^2 of buried hydrophobic ASA derived from the ΔC_p estimate of Lee and Timasheff (1977; see Table 1), although we cannot necessarily assign that entire area as a hydrophobic surface, because $\Delta A_T = \Delta A_P + \Delta A_{NP}$. The Lee and Timasheff (1977) estimate is approximately 90% larger than our estimates of ΔA_{NP} under GTP-2 M glycerol and taxol conditions. If the buried ΔA_p is 60% of the buried ΔA_{NP}, as assumed in our calculations, then based upon this estimate of ΔA_T, the total buried nonpolar ASA, ΔA_{np}, is 3224 Å^2. This value is in excellent agreement with our estimate of 3330 ± 820 Å^2 derived from an average of assembly studies done with GTP-2 M glycerol and with taxol/GTP/GDP.

If we average the ΔC_p estimates from Lee and Timasheff (1977) with the Zn sheet data of Melki and Carlier (1993) and the colchicine data from Andreu et al. (1983), we derive an average estimate of total buried hydrophobic surface of 5580 ± 333 Å^2. (We recognize that this is an arbitrary grouping, but we will utilize this to develop a rationale for the factors that might contribute to ΔA_T.) Although this estimate is larger than our calculated ΔA_{NP}, it is possible the additional area, approximately 2250 Å^2, is derived from conformational changes upon assembly under those experimental conditions that induce the burial of nonpolar surface. The agreement between these measurements is interesting for a number of reasons. Zinc induces sheets with alternating protofilaments that run in opposite polarity and that are inverted relative to one another, i.e., the outside surface in a microtubule lattice is up in one protofilament and down in the next. Colchicine induces a significant change in the microtubule lattice, causing an elongated sheetlike structure to be formed. Furthermore, colchicine induces a weak GTPase activity in the tubulin heterodimer (Andreu et al., 1983). One might suspect this conformational change would make the tubulin heterodimer more similar to the polymerized subunit and thus minimize that contribution to the thermodynamics. The fact that the colchicine data are an outlier in our ΔH-ΔG plot (Fig. 5 *B*) seems to support this expectation. Thus, although a similarity in the thermodynamics under these conditions seems fortuitious, we must conclude that these processes proceed by similar driving forces that are entropic in nature and dominated by the hydrophobic effect, as demonstrated by a large negative ΔC_p. The larger estimates from these data for

ΔA_{NP} (5580 ± 333 Å^2) compared to our GTP-2 M glycerol and taxol data (3330 ± 820 Å^2) are not unreasonable, given the experimental uncertainty and the overlap between the ΔC_p data sets. The data derived from the GMPCPP-induced assembly (9220 ± 2180 Å^2) are approximately twofold larger, but again because of the experimental overlap with the Lee and Timasheff data (1977, Table 1) and the uncertainty in the ratio of $\Delta A_P/\Delta A_{NP}$, it is not an unreasonable estimate. However, the estimate with GMPCP-induced assembly (22,250 ± 4,760 Å^2) does seem large. To evaluate this we calculated the entire hydrophobic surface available in the tubulin heterodimer amino acid sequence. Using the amino acid sequences of porcine α- and β-tubulin (Ponstingl et al., 1981; Krauhs et al., 1981), we summed the total hydrophobic surface in each amino acid based upon the Gly-X-Gly data of Richards (1977). This gives a total of 84,400 Å^2. The majority of this hydrophobic surface is expected to be buried upon tubulin folding and heterodimer formation. The GMPCP-derived estimate of ΔA_{NP} corresponds to 26% (± 5.6%) of the total available surface area in tubulin. (This rather large and unreasonable value is quantitatively evaluated below after a discussion of entropy analysis.)

Entropy analysis of thermodynamic data

To further quantitatively access these data, we attempted to partition the entropy into contributions from the hydrophobic effect (ΔS_{HE}), the loss of rotational/translational freedom (ΔS_{RT}), and the loss of conformational entropy (ΔS_{OTHER}) (Table 3). By utilizing the method outlined by Spolar and Record (1994), ΔS_{HE} can be estimated from ΔC_P at T_S, the temperature at which $\Delta S = 0 = \Delta S_{HE} + \Delta S_{RT} + \Delta S_{OTHER}$. For the microtubule polymerization reactions summarized in Table 1 that have a nonzero ΔC_P, we observe an average T_S = 317.6 ± 7.7. This variation is typical of other comparisons (Spolar and Record, 1994), and using this average value has no effect on the qualitative or quantitative conclusions of this analysis. ΔS_{HE} can then be estimated at T_S by the relationship $\Delta S_{HE}(T_S) = 1.35 * \Delta C_P * \ln(T_S/386)$ (Baldwin, 1986; Spolar and Record, 1994). These values are presented in Table 3 and, as expected, reflect significant variation proportional to the variation in ΔC_P. If we assume that all association reactions involve a comparable loss of rotational/translational freedom, ΔS_{RT} = −50 eu, regardless of the number of contacts or interfaces formed per subunit (Spolar and Record, 1994), then ΔS_{OTHER} can be estimated at T_S by the null relationship. (The use of −50 eu for ΔS_{RT} is in reasonable agreement with the results of other authors (Spolar and Record, 1994). Frigon and Timasheff (1975b) estimated a value of −60 eu for their analysis of Mg-induced ring formation. More recently Erickson (Erickson and Pantaloni, 1981; Erickson, 1989) estimated a value of 25–36 eu for $-\Delta S_{RT}$ in an analysis of the assembly of tubulin and the assembly of actin. In both of these studies he assumed rigid-body association and thus ignored any contribution from ΔS_{OTHER}. Horton and Lewis (1992) attempted to estimate ΔS_{RT} from an analysis of the nonpolar and polar character of crystal structure interfaces. For complexes that appeared to undergo rigid-body association, they estimated ΔS_{RT} to be 20.7 eu, corresponding to 6.2 ± 2.2 kcal/mol. Because ΔS_{RT} is, in general, 2–26-fold smaller than ΔS_{OTHER}, and 3–15-fold smaller, in absolute value, than ΔS_{HE} (Table 3), our use of −50 eu for ΔS_{RT} is extremely reasonable and will affect each estimate of ΔS_{OTHER} by the same small magnitude, corresponding to no more than six amino acid residues.) ΔS_{OTHER} has been interpreted as corresponding to loss of configurational entropy due to conformational changes driven by binding energy. In the case of DNA binding proteins, this has been interpreted as disorder-order transitions that are induced by site-specific DNA binding (Spolar and Record, 1994). For rigid-body associations that do not involve induced conformational changes, ΔS_{OTHER} will be 0, whereas for net folding reactions $\Delta S_{OTHER} < 0$, and thus will be unfavorable.

Table 3 presents a summary of this entropic analysis. As expected from the ΔC_p data, all microtubule polymerization reactions are driven by large positive entropy terms corresponding to the hydrophobic effect. (The only exception in Table 1 corresponding to Mg-induced ring formation (Frigon and Timasheff, 1975a,b) is where a small positive ΔC_P and ΔS_{OTHER} correspond to a net favorable unfolding upon ring formation.) Polymerization induced by GTP-2 M glycerol is very similar to microtubule assembly induced by taxol. Both processes exhibit a large ΔS_{HE} term (208 ± 51 eu) corresponding to the release of water. Correcting for the loss of rotational/translational freedom gives an average ΔS_{OTHER} value of −158 ± 51 eu for these two groups of data. Although the ΔS_{OTHER} from individual groups are very similar (−169 ± 50 eu for the GTP/2 M glycerol data and −142 ± 49 eu for the taxol/GDP/GTP data), the spread of the data is large (−93 to −235 eu), consistent with the error in ΔC_p. These values correspond to disorder-order transition or folding reactions induced by assembly. How many amino acids might be involved in this conformational change? Spolar and Record (1994) have suggested that if changes in secondary and tertiary structure dominate ΔS_{OTHER}, then each amino acid will contribute −5.6 eu to the transition. This corresponds to 28 ± 9 amino acids (designated R^{th} in Table 3) or approximately 3.1% of the total residues in the tubulin hetrodimer, a rather small value considering the number of interfaces and the estimated contact surface area in a microtubule lattice. The data of Lee and Timasheff (1977) give an estimate for ΔS_{OTHER} (345 eu) and R^{th} (62) that is twice as large, whereas the average values of the data from other laboratories (Lee and Timasheff, 1977; Melki and Carlier, 1993; Andreu et al., 1983) are 299 ± 34 eu for ΔS_{OTHER} and 53 ± 6 for R^{th}. This corresponds to approximately 6% of the total residues in the dimer and, given the uncertainty in the measurements, allows us to conclude that microtubule assembly induced by a variety of ligands (GTP, taxol, Zn, colchicine) involves

loss of conformational entropy in 3–6% of the total amino acid residues. Utilizing Raman spectroscopy, Audenaert et al. (1989) compared the secondary stucture of tubulin heterodimers with the structure of microtubules and found a decrease in ordered and disordered α-helix (7% and 2%, repectively) and a 7% increase in β-sheet upon assembly of GTP-tubulin into microtubules. This suggests that the conformational changes implied by ΔS_{OTHER} do not necessarily mean secondary structure formation from random coil, but might correspond to a decrease in mobility or an ordering of existing secondary structure elements.

Polymerization with GMPCPP suggests larger average values for ΔS_{OTHER} and R^{th} (526 ± 136 and 94 ± 24, respectively), although the wide spread in the data (for example, R^{th} varies from 62 to 121 residues) leaves some uncertainty as to the significance of these trends. These average values correspond to approximately 10% of the total residues. Polymerization with GMPCP suggests that more than 25% of the residues undergo a disorder-order transition upon assembly. This value is too large to correspond to a random coil-to-secondary structure transition, because the undefined secondary structure predicted for the tubulin heterodimer is only 10–12% (Lee and Timasheff, 1977; Audenaert et al., 1989). For this value to be accurate, GMPCP must either be inducing significant disorder in the tubulin heterodimer, and/or dramatically inducing more order in the assembled structure. GMPCP does not induce significant unfolding in the tubulin heterodimer, because under nonpolymerizing conditions the sedimentation coefficient of GMPCP-tubulin is identical to that of GDP- and GTP-tubulin (Vulevic and Correia, manuscript in preparation).

What can we conclude about these large discrepancies in estimated buried ASA, ΔS_{OTHER}, and R^{th} values? Within the experimental error, our results with GTP/2 M glycerol- and taxol-induced assembly are in reasonabe agreement with the results of Lee and Timasheff (1977), Melki and Carlier (1993), and Andreu et al. (1983). Although the average values differ by a factor of 2, there is significant overlap at the 65% confidence interval. Nonetheless, the Lee and Timasheff (1977) and the Andreu et al. (1983) data were collected with tubulin purified by a different method in a PO_4 buffer with 16 mM $MgCl_2$ and 3.4 M glycerol. At 16 mM $MgCl_2$ tubulin forms rings (Frigon and Timasheff, 1975a,b), and thus microtubule assembly in those cases partially involves dissociation of structures that have less order (ΔS_{OTHER} = +147 for ring formation) than heterodimers into microtubule polymers that are more ordered. Note that the difference in ordered amino acids between our average data (R^{th} = 28 ± 9) and the average data from these other laboratories (R^{th} = 53 ± 6) is exactly the number of disordered amino acids that form upon ring formation (R^{th} = 26). That ring formation competes with microtubule assembly at high Mg^{2+} concentrations has recently been verified by Diaz et al. (1996). The small positive heat capacity change seen in Mg^{2+}-induced ring formation might be due to Mg^{2+}-induced burial of polar surface. Mg^{2+} is required for microtubule assembly, partially for GTP binding (Correia et al., 1987), but also for overcoming charge-charge repulsion in the acidic carboxyl tail of both subunits (Diaz et al., 1993). Based upon these arguments, the effect of different buffer conditions on changes in heat capacity can be attributed to 1) unique conformational changes that induce buried polar or nonpolar ASA, and 2) alternative coupled polymerization reactions that contribute to the overall thermodynamics. (To verify these conclusions, we performed van't Hoff analysis of microtubule assembly in the Lee and Timasheff (1977) buffer with PC-tubulin. The addition of 3.4 M glycerol precluded collecting data below 25°C because of the additional dilution of tubulin, but we were able to obtain enough data (not shown because of the large uncertainty) to estimate a ΔC_P of −1470 ± 1250 cal/mol/K, a ΔH of 13.9 ± 7.0 kcal/mol, and a ΔS of 69 ± 23 cal/mol/K. This ΔC_P value is nearly identical to the estimate of Lee and Timasheff (1977; Table 1) and supports our suggestion that the observed differences are due to different buffer conditions.)

Our experiments with GMPCPP and GMPCP were done in essentially the same buffer as our GTP-2 M glycerol and taxol experiments. Thus, buffer effects cannot explain the discrepancies of three to five times ΔC_p, ΔS_{OTHER}, and R^{th} between these data. Hyman et al. (1995) observed an increase in the subunit spacing along a protofilament of GMPCPP-induced microtubules of 1.5 Å/subunit. Thus, GMPCPP-tubulin assembly must induce extensive conformational rearrangements that either cause burial of more nonpolar ASA or less polar ASA to accommodate this more extended structure. It is assumed that these rearrangements reflect the structure of GTP microtubules (Vale et al., 1994; Hyman et al., 1995). The additional increase of two to three times induced by GMPCP, as discussed above, must cause more extensive conformational rearrangements in the polymer. This suggests that the differences with GMPCPP and GMPCP are due to a nucleotide effect, possibly suggesting that GMPCPP is not a true, isomorphous GTP analog. This conclusion hinges upon the interpretation of the GMPCP data. One alternative interpretation is that GMPCP-tubulin is more prone to denaturation at higher temperatures, thus causing a smaller apparent C_r and the observed curvature. We do not favor this interpretation, because the turbidity is completely reversible with GMPCP-tubulin. Bundling could also bury ASA, estimated at one to two protofilaments worth of surface area along the length of a bundle. However, we have no evidence of extensive bundling under any of our solution conditions. It is also possible that the -CH_2- group in GMPCP induces additional protonation/deprotonation or isomerization events that contribute to the observed curvature (Eftink et al., 1983). Given the extremely large ΔC_p observed for GMPCP-induced assembly, we favor this interpretation. This interpretation is consistent with the observations of Vale et al. (1994) and Hyman et al. (1995) and suggests that GMPCP and GMPCPP microtubules are not isomorphous with GDP and GTP microtubules.

Observations of minimum heat capacity changes

A number of microtubule assembly studies reported no curvature and thus a ΔC_p of 0 (Table 1). For example, Detrich et al. (1992) report linear van't Hoff data over the range of 0–19°C for two Antarctic fish tubulins. Because the majority of the other data span a higher temperature range, it is possible that this result is due to a difference in abscissa. To test this we simulated "perfect" data with the parameters of Lee and Timasheff (1977) over the range of 0–19°C and the experimental range in Detrich et al. (1992), and then fit them to a straight line. This gave a $\Delta H°$ of 40.6 kcal/mol and a $\Delta S°$ of 160 cal/mol/K, values very similar to the results of Detrich et al. (1992) for fish egg tubulin. The linear fit had a standard deviation of 0.12, which means within the typical error for these experiments (0.06–0.30; see Table 1), and over this temperature range the data might appear linear, even though they contained a heat capacity change. (The visual observation of curvature is enhanced by the occurrence of a peak, typically occurring at approximately 37°C or the T_H temperature for these data, and thus is absent in the Detrich et al. (1992) data.) Thus the linear data of Detrich et al. (1992) are consistent with the ΔC_p values reported for microtubule assembly. However, it is also possible that Antarctic fish tubulin has a sequence that minimizes hydrophobic contibutions to allow favorable polymerization at −1.9°C and thus reflects a real change in the heat capacity relative to mammalian tubulin. Johnson (Johnson and Borisy, 1977; Johnson, 1980) reported two linear segments of a van't Hoff plot for the assembly of MAP containing microtubule protein. The lower segment spans a range similar to that of the data of Detrich et al. (1992), and thus similar arguments might be made. However, as noted above, MAPs induce oligomer formation, and thus microtubule assembly with MAPs involves changes in states of oligomerization at low temperatures and MAP binding at higher temperatures, a primarily electrostatic process. Thus the ΔC_p for these coupled processes is additive and may be concealed by the complexity of MAP binding and oligomer dissociation.

Diaz et al. (1993) observed no change in the heat capacity, 0 ± 71 kcal/mol/K, for taxol- and taxotere-induced microtubule assembly. This is in contrast to the significant ΔC_p we observe for both taxol/GTP- and taxol/GDP-induced assembly. (On an absolute scale the average difference is similar to that observed between our taxol data and the average results of other assembly studies (Lee and Timasheff, 1977; Andreu et al., 1983; Melki and Carlier, 1993).) There is a difference in the tubulin preparations used, but the major difference between the two studies is the buffer composition. Diaz et al. (1993) used 4 mM $MgCl_2$ in their assembly buffer. However, we suggested above that this might lead to a larger, not smaller, negative value of ΔC_p by the coupled dissociation of rings. We can only point out that their van't Hoff plots are adjusted to 2 mM free Mg^{2+}, pH 7.0, taking into account temperature-dependent Mg^{2+} binding by GTP, GDP, and PO_4, and dpK/dT for phosphate buffer. These corrections may introduce a decrease in curvature. All of our studies are done with 1 mM total $MgSO_4$ and PIPES buffer at pH 6.9, and thus, relative to each other, should reflect comparable changes in pH and Mg^{2+} concentration. (To directly address this discrepancy, we performed van't Hoff analysis of microtubule assembly in the Diaz et al. (1993) buffer with taxol/GTP. We experienced some difficulty in getting stable cold baselines and had to resort to adding 1 mM GTP at the start of the warm temperature jump. Note that GTP-tubulin was the starting material, prepared as described in Materials and Methods, but without excess GTP. Our analysis of the data (not shown) gave an estimate of ΔC_P of −902 ± 642 cal/mol/K, a value consistent with our average value of −790 ± 190 cal/mol/K, a ΔH of 3.8 ± 2.3 kcal/mol, and a ΔS of 38 ± 8 cal/mol/K. Thus, in our hands, microtubule assembly under all conditions exhibits a negative heat capacity change.) It is generally agreed (Lee and Timasheff, 1977; Sutherland, 1977) that the enthalpy measured in van't Hoff analysis is the enthalpy of microtubule propagation and corresponds to $K_p = 1/c_r$ (as described in Materials and Methods). Our taxol-stimulated assembly data exhibit smaller $\Delta H°$ and $\Delta S°$ values, consistent with a significant contribution from taxol binding. A similar effect is evident in the Johnson and Borisy (1979) data (>20°C), in which a contribution from MAP binding to microtubules is anticipated. The data of Diaz et al. (1993) exhibit a similar decrease in $\Delta H°$ and $\Delta S°$ relative to the data of Lee and Timasheff (1977). Thus the binding of stabilizing ligands (taxol, taxotere, and MAPs) has the expected thermodynamic effect of making the enthalpy more favorable. The compensating decrease in entropy is assumed to be due to immobilization of ligand.

Enthalpy-entropy compensation is due to real biochemical effects

Based on the elegant statistical analysis of Krug et al. (1976a,b,c), we have demonstrated that microtubule formation and numerous tubulin self-association reactions exhibit reliable enthalpy-entropy compensation. This allows us to conclude that these self-association reactions reflect similar protein-protein interactions. A more chemical, mechanistic interpretation of enthalpy-entropy compensation has been offered by Dunitz (1995) for weak intermolecular interactions involving small ligands. As affinity increases by increasing enthalpic interactions, the ligand(s) are increasingly immobilized in the site, thus increasing their entropy. For macromolecular interactions the role of solvent becomes more critical, especially for large interaction interfaces, where the release of bound water from buried hydrophobic surfaces clearly contributes significant enthalpy and entropy changes to the system. Spolar and co-workers (Ha et al., 1989; Spolar and Record, 1994) have demonstrated that a consequence of a large negative heat capacity change is that the enthalpy and entropy contributions to ΔG vary with temperature in a nearly parallel manner.

Swezey and Somero (1982, 1985) observed a similar enthalpy-entropy compensation for the self-association of skeletal muscle actins from 14 vertebrate species. The covariance exhibited a compensation temperature (T_c = 275 K) remarkably similar to what is observed with tubulin assembly (278.1 ± 6.3 K). Note that for these data the mean harmonic temperature was only 15°C, versus 27°C in our data. Swezey and Somero (1982, 1985) made two suggestions for the mechanism of compensation in actin filament formation. First they proposed that an alteration in the types of bonds at intersubunit contacts between species (i.e., hydrophobic versus charged) caused a variation in the contribution from release of water upon protein-protein interaction. In our data and all but two cases reported for tubulin (Table 1), mammalian brain protein was used, and thus this interpretation could only arise if other factors like ligand binding contributed to alterations in intersubunit contacts. In addition, it was suggested that an alteration in the energetic cost of a conformational change upon filament formation occurred between species. The conformational change in actin is hypothesized to occur before filament formation, i.e., G → G* → F. Energetically this is analogous to a conformational change after polymerization and may in fact account for variations in stabilizing forces that are linked to GTP hydrolysis or ligand binding. Nonetheless, we conclude that the dominant contribution to enthalpy-entropy compensation in microtubule assembly is the hydrophobic effect and the burial of nonpolar-accessible surface area.

Structural studies and the relationship between nucleotide content and microtubule closure

Our analysis confirms a linkage between GTP hydrolysis and sheet closure. Polymerization in GMPCP-2 M glycerol revealed an extremely low level of sheetlike structures, approximately 1% of the total length and <1% of the total microtubules. Consistent with the occurrence of hydrolysis in a GTP ± 2 M glycerol assembly system, we observed 1.7–2.5% of the total length in sheets. Polymerization in the presence of the weakly hydrolyzable analog GMPCPP revealed 6.9% of the total length in sheet. This was verified in a 2 M glycerol control experiment if greater time was allowed for microtubule closure. These data are consistent with a weak energetic linkage between nucleotide content, GTP hydrolysis, and sheet closure, i.e., the stability of the microtubule seam. Diaz et al. (1996) inferred a similar linkage between nucleotide content and the relative stability of GDP-tubulin rings and taxol-induced microtubules. They discussed this linkage as an equilibrium between a curved GDP-tubulin ring and a straight taxol-stabilized microtubule conformation, and outlined a scheme that suggested competing equilibria between Mg^{2+}-dependent rings, sheets of rings, and microtubules. They also observed by solution x-ray scattering a slow phase during taxol-induced assembly that involved sheet closure into a microtubule lattice. Although the slow phase was only 500-1500 s, it represented 15–20% of the total scattering signal. This is considerably faster than GMPCPP-2 M glycerol-induced microtubule closure, but it is consistent with our general hypothesis. The observation of sheets as intermediates in assembly by cryoelectron microscopy (Chretien et al., 1995) and by x-ray solution scattering (Diaz et al., 1996) confirms similar kinetic observations by others (Detrich et al., 1985; Mandelkow et al., 1991; Simon and Salmon, 1990). Under these rapid growth conditions sheet extensions as long as 3–6 μm were observed, indicating that closure is rate limiting. Under disassembly conditions microtubules typically appeared blunt, although cold-induced disassembly does induce sheet formation. These prior observations in conjunction with the clear differences we report (Table 1) suggest that sheet polymers are not artifacts of negative stain EM. It is possible that the EM technique contributed to breaks along the seam; however, the nucleotide and time-dependent differences we observe clearly suggest energetic linkages between nucleotide content, GTP hydrolysis, and the stability of a closed microtubule seam. Thus our observations with equilibrium and nondynamic microtubules suggest that an equilibrium also exists between sheet polymers and microtubules (Table 2).

The additional observation that sheet polymers are an average length of 404 ± 99 nm is consistent with a cooperative mechanism of closure. Estimation of an equilibrium contant for the process based upon the percentage data or upon length distribution data is complicated because a cooperative process of this type necessarily involves a nucleation of seam breakage and a propagation of that break. Any mechanism must also take into account the geometrical constraints of the minimum length of seam breakage that allows a microtubule to open and spread on the grid. Nonetheless, in general the small amount of sheet present in the solution conditions studied by van't Hoff analysis suggests that the differences observed in the thermodynamics are not due to differences in the mixture of sheet and microtubule polymers. However, the inferred difference in the energetics of seam stability does suggest that the thermodynamic difference is in part due nucleotide-linked conformational changes in the lattice.

We thank National Cancer Institute for providing taxol, Jeff Turner for his technical assistance with the synthesis of GMPCP and GMPCPP, Dr. Tim Mitchison for providing the synthesis procedure, Drs. Sharon Lobert and Brad Chaires for illuminating discussion throughout this work, Dr. Ken Downing for providing a preliminary analyis of the buried ASA in a reconstructed microtubule, and the Pelahatchie Country Meat Packers for providing pig heads for tubulin purification. We especially thank Dr. Serge N. Timasheff and co-workers for their remarkable contribution to thermodynamics. Their manuscripts have been a great source of insight and education, and without their efforts our work would not have been possible.

This paper was offered in partial fulfillment of the requirements for the degree of Doctor of Philosophy in the Department of Biochemistry, University of Mississippi Medical Center (BV).

REFERENCES

Andreu, J. M., T. Wagenknecht and S. N. Timasheff. 1983. Polymerization of the tubulin-colchicine complex: relation to microtubule assembly. *Biochemistry.* 22:1556–1566.

Audenaert, R., L. Heremans, K. Heremans, and Y. Engelborghs. 1989. Secondary structure analysis of tubulin and microtubules with Raman spectroscopy. *Biochim. Biophys. Acta.* 996:110–115.

Baldwin, R. L. 1986. Temperature dependence of the hydrophobic interactions in protein folding. *Proc. Natl. Acad. Sci. USA.* 83:8069–8072.

Berkowitz, S. A., G. Veliceleb, J. W. H. Sutherland, and J. M. Sturtevant. 1980. Observation of an exothermic process associated with the in vitro polymerization of brain tubulin. *Proc. Natl. Acad. Sci. USA.* 77: 4425–4429.

Berne, B. J. 1974. Interpretation of the light scattering from long rods. *J. Mol. Biol.* 89:755–758.

Caplow, M. 1992. Microtubule dynamics. *Curr. Opin. Cell Biol.* 4:58–65.

Caplow, M., R. L. Ruhlen, and J. Shanks. 1994. The free energy for hydrolysis of a microtubule-bound nucleotide triphosphate is near zero: all of the free energy for hydrolysis is stored in the microtubule lattice. *J. Cell Biol.* 127:779–788.

Caplow, M., and J. Shanks. 1996. Evidence that a single monolayer tubulin-GTP cap is both necessary and sufficient to stabilize microtubules. *Mol. Biol. Cell.* 7:663–675.

Carlier, M.-F., D. Didry, and D. Pantaloni. 1987. Microtubule elongation and guanosine 5′-triphosphate hydrolysis. Role of guanine nucleotides in microtubule dynamics. *Biochemistry.* 26:4428–4437.

Chaires, J. B. 1996. Possible origin of differences between van't Hoff and calorimetric enthalpy estimates. *Biophys. Chem.* (in press).

Chretien, D., S. D. Fuller, and E. Karsenti. 1995. Structure of growing microtubule ends: two dimensional sheets close into tubes at variable rates. *J. Cell Biol.* 129:1311–1328.

Correia, J. J., L. T. Baty, and R. C. Williams, Jr. 1987. Mg^{2+} dependence of guanine nucleotide binding to tubulin. *J. Biol. Chem.* 262: 17278–17284.

Correia, J. J., and J. B. Chaires. 1994. Analysis of drug-DNA binding isotherms: a Monte Carlo approach. *Methods Enzymol.* 240:593–614.

Correia, J. J., and R. C. Williams, Jr. 1983. Mechanism of assembly and disassembly of microtubules. *Annu. Rev. Biophys. Bioeng.* 12:211–235.

Correia, J. J., and D. A. Yphantis. 1992. Equilibrium sedimentation in short solution columns. *In* Analytical Ultracentrifugation in Biochemistry and Polymer Science. S. E. Harding, A. J. Rowe, and J. C. Horton, editors. Royal Society of Chemistry, Cambridge. 231–252.

Cross, A. R., and R. C. Williams, Jr. 1991. Kinky microtubules: bending and breaking induced by fixation in vitro with gluteraldehyde and formaldehyde. *Cell Motil. Cytoskel.* 20:272–278.

Detrich, H. W., III, T. J. Fitzgerald, J. H. Dinsmore, and S. P. Marchese-Ragona. 1992. Brain and egg tubulins from Antarctic fishes are functionally and structurally distinct. *J. Biol. Chem.* 267:18766–18775.

Detrich, H. W., III, M. A. Jordan, L. Wilson, and R. C. Williams, Jr. 1985. Mechanism of microtubule assembly. Changes in polymer structure and organization during assembly of sea urchin egg tubulin. *J. Biol. Chem.* 260:9479–9490.

Detrich, H. W., III, and R. C. Williams, Jr. 1978. Reversible dissociation of $\alpha\beta$ dimer of tubulin from bovine brain. *Biochemistry.* 17:3900–3907.

Diaz, J. F., J. M. Andreu, G. Diakun, E. Towns-Andrews, and J. Bordas. 1996. Structural intermediates in the assembly of taxoid-induced microtubules and GDP-tubulin rings: time-resolved X-ray scattering. *Biophys. J.* 70:2408–2420.

Diaz, J. F., M. Menendez, and J. M. Andreu. 1993. Thermodynamics of ligand-induced assembly of tubulin. *Biochemistry.* 32:10067–10077.

Drechsel, D. N., and M. W. Kirschner. 1994. The minimum GTP cap required to stabilize microtubules. *Curr. Biol.* 4:1053–1061.

Dunitz, J. D. 1995. Win some, lose some: enthalpy-entropy compensation in weak intermolecular interactions. *Curr. Biol.* 2:709–712.

Dye, R. B., and R. C. Williams, Jr. 1996. Assembly of microtubules from brain tubulin bearing the nonhydrolyzable guanosine triphosphate analogue GMPPCP [guanyl 5′-(B,γ-methylenediphosphonate)]: variability of growth rates and the hydrolysis of GTP. *Biochemistry.* 35: 14331–14339.

Eftink, M. R., A. C. Anusiem, and R. L. Biltonen. 1983. Enthalpy-entropy compensation and heat capacity changes for protein ligand interactions: general thermodynamic models and data for the binding of nucleotides to ribonuclease. *Biochemistry.* 22:3884–3896.

Erickson, H. P. 1989. Cooperativity in protein-protein association. The structure and stability of actin filaments. *J. Mol. Biol.* 206:465–474.

Erickson, H. P., and D. Pantaloni. 1981. The role of subunit entropy in cooperative assembly. Nucleation of microtubules and other two-dimensional polymers. *Biophys. J.* 34:292–309.

Frigon, R. P., and S. N. Timasheff. 1975a. Magnesium-induced self-association of calf brain tubulin. I. stoichiometry. *Biochemistry.* 14: 4559–4566.

Frigon, R. P., and S. N. Timasheff. 1975b. Magnesium-induced self-association of calf brain tubulin. I. thermodynamics. *Biochemistry.* 14: 4567–4573.

Gaskin, F., C. R. Cantor, and M. L. Shelanski. 1974. Turbidimetric studies of the in vitro assembly and disassembly of porcine neurotubules. *J. Mol. Biol.* 89:737–755.

Geahlen, R. L., and B. E. Haley. 1979. Use of a GTP photoaffinity probe to resolve aspects of the mechanism of tubulin polymerization. *J. Biol. Chem.* 254:11982–11987.

Gildersleeve, R. F., A. R. Cross, K. E. Cullen, A. P. Fagen, and R. C. Williams, Jr. 1992. Microtubules grow and shorten at intrinsically variable rates. *J. Biol. Chem.* 267:7995–8006.

Glasstone, S. G. 1947. Thermodynamics for Chemists. Van Nostrand, New York. 292–295.

Ha, J.-H., R. S. Spolar, and M. T. Record. 1989. Role of the hydrophobic effect in stability of site-specific protein-DNA complexes. *J. Mol. Biol.* 209:801–816.

Hinz, H.-J., M. J. Gorbunoff, B. Price, and S. N. Timasheff. 1979. Heat capacity microcalorimetry of the in vitro reconstitution of calf brain microtubules. *Biochemistry.* 18:3084–3089.

Horio, T., and H. Hotani. 1986. Visualization of the dynamic instability of individual microtubules by dark-field microscopy. *Nature.* 321: 605–607.

Horton, N., And M. Lewis. 1992. Calculation of the free energy of association for protein complexes. *Protein Sci.* 1:169–181.

Howard, W. D., and S. N. Timasheff. 1986. GDP state of tubulin: stabilization of double rings. *Biochemistry.* 25:8292–8300.

Hyman, A. A., D. Chretien, I. Arnal, and R. H. Wade. 1995. Structural changes accompanying GTP hydrolysis in microtubules: information from slowely hydrolyzable analogue guanylyl-(α, β)-methylene-diphosphonate. *J. Cell Biol.* 128:117–125.

Hyman, A. A., S. Salser, D. N. Drechsel, N. Unwin, and T. J. Mitchison. 1992. Role of GTP hydrolysis in microtubule dynamics: information from a slowly hydrolyzable analogue, GMPCPP. *Mol. Biol. Cell.* 3:1155–1167.

Johnson, K. A. 1980. Thermodynamics of microtubule assembly. *Biophys. J.* 32:443–445.

Johnson, K. A., and G. G. Borisy. 1979. Thermodynamic analysis of microtubule self-assembly in vitro. *J. Mol. Biol.* 133:199–216.

Kirschner, M. W. 1978. Microtubule assembly and nucleation. *Int. Rev. Cytol.* 54:1–71.

Kowalski, R. J., and R. C. Williams, Jr. 1993. Microtubule-associated protein 2 alters the dynamic properties of microtubule assembly and disassembly. *J. Biol. Chem.* 268:9847–9855.

Krauhs, E., M. Little, T. Kempf, R. Hofer-Warbinek, W. Ade, and H. Ponstingl. 1981. Complete amino acid sequence of β-tubulin from porcine brain. *Proc. Natl. Acad. Sci. USA.* 78:4156–4160.

Krug, R. R., W. G. Hunter, and R. A. Grieger. 1976a. Enthalpy-entropy compensation. 1. Some fundamental statistical problems associated with the analysis of van't Hoff and Arrhenius data. *J. Phys. Chem.* 80: 2335–2341.

Krug, R. R., W. G. Hunter, and R. A. Grieger. 1976b. Enthalpy-entropy compensation. 2. Separation of the chemical from the statistical effect. *J. Phys. Chem.* 80:2341–2351.

Krug, R. R., W. G. Hunter, and R. A. Grieger. 1976c. Statistical interpretation of enthalpy-entropy compensation. *Nature.* 261:566–567.

Lee, J. C., and S. N. Timasheff. 1977. In vitro reconstitution of calf brain microtubules: effect of solution variables. *Biochemistry.* 16:1754–1764.

Livingstone, J. R., R. S. Spolar, and M. T. Record. 1991. Contribution to the thermodynamics of protein folding from the reduction in water-accessible nonpolar surface area. *Biochemistry.* 30:4237–4244.

Mandelkow, E. M., E. Mandelkow, and R. Milligan. 1991. Microtubule dynamics and microtubule caps: a time-resolved cryo-electron microscopy study. *J. Cell Biol.* 114:977–991.

Margolis, R. L., and L. Wilson. 1978. Opposite end assembly and disassembly of microtubules at steady state in vitro. *Cell.* 13:1–8.

Martin, S. R., M. J. Schilstra, and P. M. Bayley. 1993. Dynamics instability of microtubules: Monte Carlo simulation and application to different types of microtubule lattice. *Biophys. J.* 65:578–596.

Melki, R., and M.-F. Carlier. 1993. Thermodynamics of tubulin polymerization into zinc sheets: assembly is not regulated by GTP hydrolysis. *Biochemistry.* 32:3405–3413.

Melki, R., M.-F. Carlier, D. Pantaloni, and S. N. Timasheff. 1989. Cold depolymerization of microtubules to double rings: geometric stabilization of assemblies. *Biochemistry.* 28:9143–9152.

Mitchison, T. J., and M. Kirschner. 1984. Dynamic instability of microtubule growth. *Nature.* 312:237–242.

Murphy, K. P., P. L. Privalov, and S. J. Gill. 1990. Common features of protein unfolding and dissolution of hydrocarbon compounds. *Science.* 247:559–561.

Nogales, E., S. G. Wolf, I. A. Khan, R. F. Luduena, and K. H. Downing. 1995. Structure of tubulin at 6.5 Å, and location of taxol-binding site. *Nature.* 375:424–427.

Penefsky, H. S. 1977. Reversible binding of P_i by beef heart mitochondrial adenosine triphosphatase. *J. Biol. Chem.* 252:2891–2899.

Ponstingl, H., E. Krauhs, M. Little, and T. Kempf. 1981. Complete amino acid sequence of α-tubulin from porcine brain. *Proc. Natl. Acad. Sci. USA.* 78:2757–2761.

Richards, F. M. 1977. Area, volumes, packing and protein structure. *Annu. Rev. Biophys. Bioeng.* 6:151–176.

Ross, P. D., and S. Subramanian. 1981. Thermodynamics of protein association reactions: forces contributing to stability. *Biochemistry.* 20: 3096–3102.

Seckler, R., G. M. Wu, and S. N. Timasheff. 1990. Interactions of tubulin with guanylyl-(beta-gamma-methylene) diphosphonate. Formation and assembly of a stoichiometric complex. *J. Biol. Chem.* 265:7655–7661.

Serrano, L., J. De la Torre, R. B. Maccioni, and J. Avila. 1984. Involvement of the carboxyl-terminal domain of tubulin in the regulation of its assembly. *Proc. Natl. Acad. Sci. USA.* 81:5989–5993.

Simon, J. R., and E. D. Salmon. 1990. The structure of microtubule ends during the elongation and shortening phases of dynamic instability examined by negative-stain electron microscopy. *J. Cell Sci.* 96: 571–582.

Spolar, R. S., J.-H. Ha, and M. T. Record. 1989. Hydrophobic effect in protein folding and other noncovalent processes involving proteins. *Proc. Natl. Acad. Sci. USA.* 86:8382–8385.

Spolar, R. S., J. R. Livingstone, and M. T. Record. 1992. Use of liquid hydrocarbon and amide transfer data to estimate contributions to thermodynamic functions of protein folding from the removal of nonpolar and polar surface from water. *Biochemistry.* 31:3947–3955.

Spolar, R. S., and M. T. Record. 1994. Coupling of local folding to site-specific binding of proteins to DNA. *Science.* 263:777–784.

Stewart, R. J., K. W. Farrell, and L. Wilson. 1990. Role of GTP hydrolysis in microtubule polymerization: evidence for a coupled hydrolysis mechanism. *Biochemistry.* 29:6489–6498.

Sturtevant, J. M. 1977. Heat capacity and entropy changes in processes involving proteins. *Proc. Natl. Acad. Sci. USA.* 74:2236–2240.

Sutherland, J. W. H. 1977. Disagreement between calorimetric and van't Hoff enthalpies of assembly of protein supramolecular structures. *Proc. Natl. Acad. Sci. USA.* 74:2002–2006.

Sutherland, J. W. H., and J. M. Sturtevant. 1976. Calorimetric studies of the in vitro polymerization of brain tubulin. *Proc. Natl. Acad. Sci. USA.* 73:3565–3569.

Swezey, R. R., and G. N. Somero. 1982. Polymerization thermodynamics and structural stabilities of skeletal muscle actins from vertebrates adapted to different temperatures and hydrostatic pressures. *Biochemistry.* 21:4496–4503.

Swezey, R. R., and G. N. Somero. 1985. Pressure effects on actin self-assembly: interspecific differences in the equilibrium and kinetics of the G to F transformation. *Biochemistry.* 24:852–860.

Timasheff, S. N., and L. M. Grisham. 1980. In vitro assembly of cytoplasmic microtubules. *Annu. Rev. Biochem.* 49:565–591.

Vale, R. D., C. M. Coppin, F. Malik, F. J. Kull, and R. A. Milligan. 1994. Tubulin GTP hydrolysis influences the structure, mechanical properties, and kinesin driven transport of microtubules. *J. Biol. Chem.* 269: 23769–23775.

Venier, P., A. C. Maggas, M.-F. Carlier, and D. Pantaloni. 1994. Analysis of microtubule rigidity using the hydrodynamic flow and thermal fluctuations. *J. Biol. Chem.* 269:13353–13360.

Vonck, J., and E. F. J. van Bruggen. 1990. Electron microscopy and image analysis of two-dimensional crystals and single molecules of alchocol oxidase from *Hansenula polymorpha. Biochim. Biophys. Acta.* 1038: 74–79.

Williams, R. C., Jr., and J. C. Lee. 1982. Preparation of tubulin from brain. *Methods Enzymol.* 85:376–408.

Wyman, J. 1964. Linked functions and reciprocal effects in hemoglobin: a second look. *Adv. Protein. Chem.* 19:223–386.

Wyman, J., And S. J. Gill. 1990. Binding and Linkage: Functional Chemistry of Biological Macromolecules. University Science Books, Mill Valley, CA.